A Stochastic Model for Estimating the Network-Scale Deterioration and Effect of Interventions on Bridges

ZACHARY HAMIDA*and JAMES-A. GOULET
Department of Civil, Geologic and Mining Engineering
POLYTECHNIQUE MONTREAL, <u>CANADA</u>

December 1, 2021

Abstract

Visual inspections provide direct information about the deterioration states of each structural element within a bridge. However, when managing a network of bridges, it becomes necessary to aggregate the deterioration information from the element-level to the bridge-level or even the network-level. Deterioration models that are based on state-space models (SSM) have the capacity to model the deterioration based on visual inspections and structural attributes. Nonetheless, the application of such models has been demonstrated at the element-level only. In this study, the SSM deterioration framework is extended to provide overall estimates for the deterioration states of bridges and of an entire network. The proposed approach also includes a framework for handling missing data and interventions. The framework's capacity is demonstrated using data from individual cases of bridges, with and without interventions, in addition to a network of $\mathtt{B} \approx 7000$ bridges in the Canadian province of Quebec. The deterioration estimates for bridges can aid in examining the effectiveness of previous interventions, the long-term trend of the network's condition, as well as laying the groundwork for planning future maintenance actions.

Keywords: Network-Scale Deterioration, Network-Scale Effect of Interventions, Visual Inspections, Inspector Uncertainty, State-Space Models, Structural Health Monitoring.

1 Introduction

Performing network-scale analyses such as prioritizing the maintenance of bridges under budgetary constraints, requires having an overall evaluation for the performance or the health state of each bridge [6, 31, 3, 9, 37]. Such evaluations can be obtained by aggregating the deterioration information of many structural elements and systems within the bridge, into a single metric. Nonetheless, the aggregation comes at the cost of some loss in information [1], therefore, it is important to consider the uncertainty associated with the estimates of the bridge's overall health state. Furthermore, structural factors (e.g., structural element size, bridge length, etc.) can have an important role in this type of analyses [33], because they can be utilized as weights, which allows prioritizing some aspects within the bridge or within the network [6].

There exists different approaches for evaluating the performance of structural systems [6, 15, 10, 34]. Reliability-based methods are among the common approaches for assessing the safety of infrastructure systems over time [34, 10, 32]. Nonetheless, such methods have a limited capacity to scale for applications involving a large network of infrastructure systems [34, 10]. This is mainly due to modelling challenges, such as defining the systems' interdependence [10], and computational challenges, such as compromising computational time versus computational resources [34]. Other methods for system-level assessment have relied directly on health monitoring data in order to evaluate the deterioration state of a structural system [6, 33, 3]. These methods have the advantage of scaling well with large infrastructure systems, in addition to being computationally inexpensive by design. The ratio-based methods rely mainly on the ratio of the deterioration state to the perfect state of structural elements [6, 17]. In this approach, the

---

*Corresponding author: zachary.hamida@polymtl.ca

sum of elements' condition is weighted by the replacement cost, which accordingly allow emphasizing the relative importance of different elements to the bridge. One of the limitations in the ratio-based approach is that it is challenging to estimate the actual replacement cost of elements which induce additional uncertainties on the overall estimate of the bridge deterioration state [6]. Other approaches for estimating the overall deterioration state of bridges suggest aggregating the deterioration states of the structural components based on weighted averaging of different importance factors. Importance factors can be assigned at the element-level to amplify the criticality of some elements in the bridge (e.g., the extent of damage in an element), or at the network-level to amplify the importance of some bridges over others (e.g., annual average of daily traffic (AADT) on a bridge). Determining the weights of importance factors is a subjective task, that mainly relies on expert judgement [6, 33, 3]. In the case where such ratios are not predefined or available, it is reasonable to consider each possible factor independently, which could convey an interpretable and specific information about the deterioration state of the network.

Even though the aforementioned methods are computationally efficient, the effectiveness of such methods is mainly dependent on the capacity to interpret the monitoring data collected over time. The health monitoring data that is commonly employed in the aforementioned methods is visual inspections data [6, 23]. Visual inspections are an element-level monitoring technique, where the elements are evaluated on-site by inspectors, over a variable time-interval (e.g., every two or three years). Although visual inspections provide direct and broad information about the deterioration condition of an element, this monitoring technique is known to be subjective, which is often reflected by a noticeable variability in the data collected over time [2, 25, 5]. Modelling the deterioration based on visual inspection data is done using different methods such as discrete Markov model (DMM) [30, 19, 20, 18, 7, 8, 35, 38], regression models [36, 16, 22], and state-space models (SSM) [11, 12, 13]. Out of these methods, the SSM deterioration model has effectively accounted for the inspectors' uncertainty, and allowed incorporating structural attributes in the deterioration analyses [12]. Nonetheless, the application of the SSM-based frameworks has been demonstrated only at the structural-element level.

In this study, the application of the SSM-based models is extended to provide the overall deterioration estimates for bridges and the network collectively. The proposed aggregation method relies on a Gaussian mixture reduction approach, where the weights are determined based on different structural factors. Furthermore, an approach for handling missing data and interventions is formulated in order to account for missing information. One of the main advantages of the proposed methods is the incorporation of the inspectors' uncertainty throughout the analyses, in addition to quantifying the deterioration speed at the bridge-level and on a network-scale, which can serve as an additional asset for planning maintenance activities. Case studies that are utilized in demonstrating the applicability of the proposed methods include, estimating the overall deterioration condition and speed for: a new bridge (without interventions), a bridge with major interventions, and a network of $\mathtt{B} \approx 7000$ bridges. Further analyses involve a comparison between costs versus the effect of interventions for a subset of bridges.

1.1   Mathematical Notations

A network of bridges is defined by the set $\mathcal{Q} = \{\mathcal{B}_1, \mathcal{B}_2, \ldots, \mathcal{B}_\mathtt{B}\}$, with each bridge $\mathcal{B}_j$ containing two groups of structural elements: primary $\mathcal{G}_1^j$ and secondary $\mathcal{G}_2^j$. The primary group $\mathcal{G}_1^j = \{\mathcal{S}_1^{j,1}, \ldots, \mathcal{S}_{\mathtt{S}_1}^{j,1}\}$, consists in structural categories that support or transfer vertical loads to other structural categories or to the ground [24]. An example of a primary structural category $\mathcal{S}_*^{j,1}$ is the category of *beam* elements. The secondary group $\mathcal{G}_2^j = \{\mathcal{S}_1^{j,2}, \ldots, \mathcal{S}_{\mathtt{S}_2}^{j,2}\}$ consists in structural categories that relate directly to the serviceability of the bridge (e.g., pavement elements). The total number of bridges in the network is $\mathtt{B}$, while $\mathtt{S}_{1:2}$ represents the total number of structural categories in each group $\mathcal{G}_{1:2}^j$. Each structural category is composed of a number of structural elements, $\mathcal{S}_m^{j,*} = \{e_1^j, e_2^j, \ldots, e_{\mathtt{E}_m}^j\}$, where e_p^j is a structural element representing the p-th element within bridge $\mathcal{B}_j$, and $\mathtt{E}_m$ is the total number of elements within a structural category $\mathcal{S}_m^{j,*}$. The health condition of each structural element is evaluated by an inspector $I_i \in \mathcal{I}$, and reported as $\tilde{y} \in [l, u]$, where l represents the worst possible condition, and u represents the best condition. Moreover, any random variable defined within the bounded space $[l, u]$, is distinguished by the symbol ($\sim$) (e.g., the observation $\tilde{y}$) [11]. It should be noted that

some notations are simplified for clarity by removing the subscript and/or the superscript. Figure 1 shows an illustration for the above-described network-scale notations (on the left side), with their corresponding deterioration states estimates (on the right side). Further details about the breakdown of the deterioration states estimates $\tilde{x}, \tilde{s}, \tilde{g}$ and $\tilde{q}$ are provided in Section §2. Other characteristics relating to the network $\mathcal{Q}$ are: the structural attributes z^j associated with each bridge $\mathcal{B}_j$, and the interventions data. The intervention data is characterized mainly by, the type of intervention h_r, the effect of the intervention δ_r and the time of intervention τ.
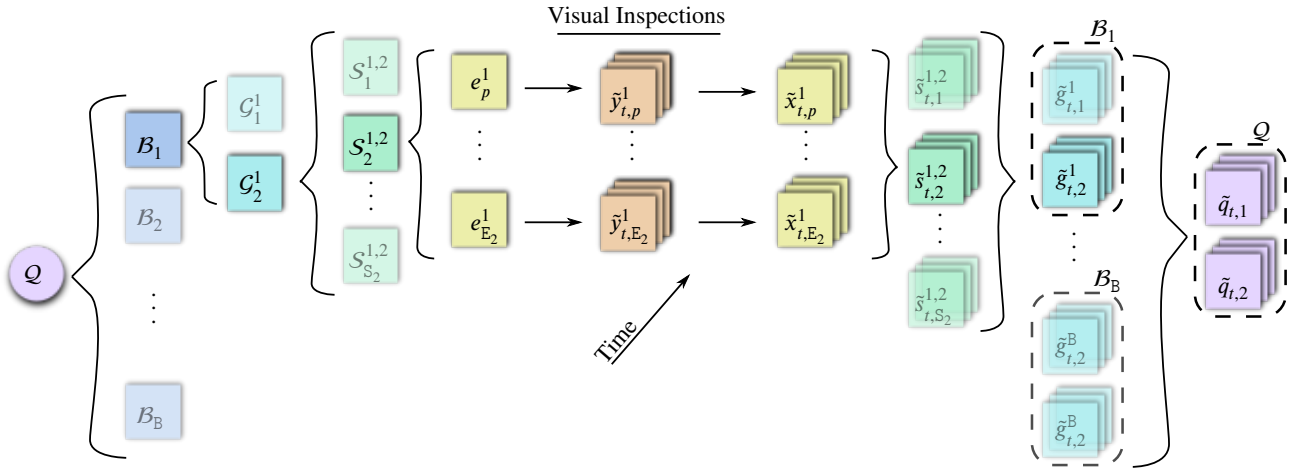

Figure 1: Hierarchy of components in the network $\mathcal{Q}$ (on the left side), with their corresponding deterioration states estimates (on the right side), and each level in the hierarchy distinguished by a unique colour. Visual inspections data $y_{t,p}^j$ are collected from the elements e_p^j over time (tilted axis), thereafter, the inspection data $\tilde{y}_{t,p}^j$ is employed to obtain the deterioration states of the elements $\tilde{x}_{t,p}^j$, which contribute to the estimation of the overall deterioration state of the category $\tilde{s}_{t,2}^{1,2}$, and similarly $\tilde{s}_{t,2}^{1,2}$ contributes to the estimation of $\tilde{g}_{t,2}^1$ in bridge $\mathcal{B}_1$, and finally $\tilde{g}_{t,2}^1$ contributes to the estimation of $\tilde{q}_{t,2}$ at the network-level.

2 Network-Scale Deterioration Analyses

Estimating the overall deterioration state of a bridge or a network follows two steps, 1) the estimation of the deterioration states at the structural element-level e_p^j, and 2) the aggregation of the deterioration states to obtain system-level state estimates. The following subsections describe the two steps in details.

2.1 Estimating the Deterioration States of Structural Elements

The deterioration analyses on structural elements are performed using a hybrid deterioration framework SSM-KR, that combines state-space models (SSM) with kernel regression (KR) [12]. The SSM describes the deterioration process using a kinematic model [4], defined by a *transition model*, and an *observation model*, The transition model describes the transition from the deterioration state $\boldsymbol{x}_{t-1,p}^j$ to the deterioration state $\boldsymbol{x}_{t,p}^j$ as in,

$$\overbrace{\boldsymbol{x}_{t,p}^j = \boldsymbol{A}_t \boldsymbol{x}_{t-1,p}^j + \boldsymbol{w}_t,}^{\text{transition model}} \underbrace{\boldsymbol{w}_t : \boldsymbol{W} \sim \mathcal{N}(\boldsymbol{w}; \boldsymbol{0}, \boldsymbol{Q}_t),}_{\text{process errors}} \tag{1}$$

where $\boldsymbol{x}_{t,p}^j : \boldsymbol{X} \sim \mathcal{N}(\boldsymbol{x}, \boldsymbol{\mu}_t, \boldsymbol{\Sigma}_t)$ is a hidden state vector at time t of element $e_p^j \in \mathcal{B}_j$. The hidden state vector $\boldsymbol{x}_{t,p}^j$ is a concatenation of two vectors, the first is $[x_{t,p}^j \ \dot{x}_{t,p}^j \ \ddot{x}_{t,p}^j]$, which describe the element's deterioration state for the condition, speed, acceleration, while the second vector describe the changes

due to interventions $[\delta_{t,p}^j \ \dot{\delta}_{t,p}^j \ \ddot{\delta}_{t,p}^j]$, for the condition, speed and acceleration respectively [13]. The matrix $\boldsymbol{A}_t$ is the state transition matrix, and $\boldsymbol{w}_t$ is the process error, with $\boldsymbol{Q}_t$ describing the process error covariance matrix. Further details about the hidden states and the transition model are provided in Appendix A.1. The second model in SSM is the observation model described by,

$$\overbrace{y_{t,p}^j = \boldsymbol{C}\boldsymbol{x}_{t,p}^j + v_t,}^{\text{observation model}} \underbrace{v_t : V \sim \mathcal{N}(v; 0, \sigma_V^2(I_i)),}_{\text{observation errors}} \tag{2}$$

where $y_{t,p}^j$ represents the observation (i.e., inspection data point), $\boldsymbol{C}$ is the observation matrix, and $v_t : V \sim \mathcal{N}(v; 0, \sigma_V^2(I_i))$, is the observation error associated with each inspector $I_i \in \mathcal{I}$, which is considered as model parameter. Estimating the hidden deterioration states is done using the *Kalman filter* (KF) [21], and the *Rauch-Tung-Striebel (RTS) Kalman smoother* (KS) [26]. Appendix A.1 provide additional details about the main equations and steps in the KF and KS frameworks. In order to ensure that the KF and KS estimates are within the inspection bounds $[l, u]$, space transformation is performed using an S-shaped transformation function $o(.)$ (see Appendix A.2) [11]. Furthermore, the monotonicity of the deterioration process is ensured by constraining the deterioration speed estimates to be negative, which is done using the PDF truncation method [29, 11].

The addition of kernel regression (KR) to the SSM framework is done to improve the overall predictive capacity by taking advantage of structural similarities across bridges [12]. More specifically, the role of KR is to provide an initial estimate for the deterioration speed $\dot{x}_{0,p}^j$ to the SSM model. This is done by recursively modelling the relation between the initial deterioration speed $\dot{x}_{0,p}^j$ and structural attributes $\boldsymbol{z}^j$ from different bridges. The procedure for estimating the parameters and hidden states related to SSM-KR is detailed in Hamida and Goulet [12]. It should be noted that if the number of structural attributes associated with a structural category $\mathcal{S}_*^{j,*}$ is limited, it can be sufficient to rely only on the SSM model without KR [12].

2.2 Estimating the Deterioration States of Structural Categories, Bridges and the Network

After estimating the deterioration states $\boldsymbol{x}_{t,p}^j$ for each structural element e_p^j at time t, the deterioration states of the elements are aggregated to obtain the overall deterioration state estimate $s_{t,m}^{j,*}$, for the structural category $\mathcal{S}_m^{j,*}$. Figure 2 shows the steps for obtaining the deterioration state $s_{t,1}^{j,1}$ of structural category $\mathcal{S}_1^{j,1} = \left\{ e_1^j, e_2^j, e_3^j \right\}$ in bridge $\mathcal{B}_j$. From Figure 2, the $\lambda_{1:3}^j$ represent the contribution of the
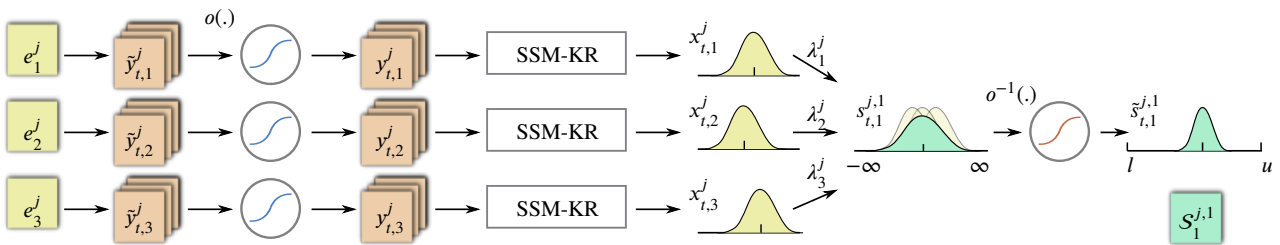

Figure 2: Steps for obtaining the deterioration state of a structural category $s_{t,1}^{j,1}$ starting from the inspection data at the element level.

deterioration state from each structural element to the overall deterioration state of the structural category $s_{t,1}^{j,1}$. The aggregation of the deterioration states is done using a Gaussian mixture reduction (GMR) approach [27, 28]. The GMR approach is employed to approximate the PDF of E_m Gaussian densities into a single Gaussian PDF [27]. The merging of the E_m Gaussian PDFs is moment-preserving,

where the total expected value $\boldsymbol{\mu}_{t|\mathtt{T},m}^{j,*}$ and the total covariance $\boldsymbol{\Sigma}_{t|\mathtt{T},m}^{j,*}$ are defined by,

$$
\begin{aligned}
\boldsymbol{\mu}_{t|\mathtt{T},m}^{j,*} &= \sum_{p=1}^{\mathtt{E}_m} \lambda_p^j \boldsymbol{\mu}_{t|\mathtt{T},p}^j, \\
\boldsymbol{\Sigma}_{t|\mathtt{T},m}^{j,*} &= \sum_{p=1}^{\mathtt{E}_m} \lambda_p^j \boldsymbol{\Sigma}_{t|\mathtt{T},p}^j + \sum_{p=1}^{\mathtt{E}_m} \lambda_p^j (\boldsymbol{\mu}_{t|\mathtt{T},p}^j - \boldsymbol{\mu}_{t|\mathtt{T},m}^{j,*})(\boldsymbol{\mu}_{t|\mathtt{T},p}^j - \boldsymbol{\mu}_{t|\mathtt{T},m}^{j,*})^{\mathsf{T}}.
\end{aligned}
\tag{3}
$$

The covariance $\boldsymbol{\Sigma}_{t|\mathtt{T},m}^{j,*}$ consists in the summation of two terms: the first term represents the within-elements contribution to the total variance, while the second term represents the between-elements contribution to the total variance [27]. In order to interpret the covariance terms, consider the example of having a structural category $\mathcal{S}_2^{j,1}$, that has all elements in a perfect condition except for one element in a bad condition. The overall expected condition for the structural category is good, however, the uncertainty about the overall expected condition will be considerably large in order to accommodate the fact that there is a large discrepancy among the elements' conditions. In the context of aggregating the deterioration states of structural elements, λ_p^j is assumed to be associated with the quantity (or the size) of the structural element d_p^j, such that, $\lambda_p^j = \frac{d_p^j}{\sum_p d_p^j}$. The quantity d_p^j is determined based on either the dimensions of the structural element (e.g., hight $\times$ width $\times$ depth) or the number of units that make up an element [24].

The process described above can be also applied for aggregating the deterioration states of the structural categories $s_{t,m}^{j,*}$ in order to obtain the deterioration state of the structural group $g_{t,*}^j$; however, λ in this case is dependent on the number of structural categories $\mathtt{S}_*$ in each group $\mathcal{G}_*^j$, such that, $\lambda_*^j = \frac{1}{\mathtt{S}_*}$. In the context of this work, the deterioration state of each bridge $\mathcal{B}_j$ is represented by the deterioration state of its primary $g_{t,1}^j$ and secondary $g_{t,2}^j$ groups (see Figure 1). This is done because the structural elements in the primary group $\mathcal{G}_1^j$ are directly associated with the safety of the bridge, while structural elements in the secondary group $\mathcal{G}_2^j$ are directly associated with the serviceability of bridge $\mathcal{B}_j$ (see Section 1.1).

Similarly, the overall deterioration state of the network is represented by $q_{t,1}$ and $q_{t,2}$, which correspond to the overall deterioration states for all elements in the primary group $\mathcal{G}_1^{1:\mathtt{B}}$ and the secondary group $\mathcal{G}_2^{1:\mathtt{B}}$, respectively. The aggregation at the network-level is based on $\lambda_j = \frac{1}{\mathtt{B}}$, where $\mathtt{B}$ is the total number of bridges in the network. Further analyses for the effect of using different λ_j on the network-scale are demonstrated in Appendix B.

3 Database: Characteristics and Processes

In this section, the main characteristics of visual inspections, intervention and bridge data are presented, along with methods for handling missing data and outliers.

3.1 Visual Inspections & Interventions Database

Visual inspections are performed on different categories of structural elements using the standard procedures described in the *inspections manual* [24]. Generally, an inspector reports the deterioration condition of a structural element using four categories of damage severity, A: *Nothing to little*, B: *Medium*, C: *Important* and D: *Very Important* [24]. An example of visual inspection data is: $y_a = 50\%$, $y_b = 30\%$, $y_c = 10\%$, $y_d = 10\%$, which implies that 50% of the structural element area has no damage, 30% has medium damage, 10% has important damage and 10% has very important damage. It should be noted that for each damage category the following conditions must apply, $0\% \le y_a, y_b, y_c, y_d \le 100\%$, and $y_a + y_b + y_c + y_d = 100\%$.

The four damage categories can be aggregated into a single metric using a weighted sum,

$$
\tilde{y} = \omega_1 y_a + \omega_2 y_b + \omega_3 y_c + \omega_4 y_d,
\tag{4}
$$

where $\omega_1 = 100$, $\omega_2 = 75$, $\omega_3 = 50$, $\omega_4 = 25$ representing the weights (or utilities), and $\tilde{y}$ is the aggregated observation [11]. Such representation allows the deterioration condition to be a

continuous numerical value with $\tilde{y} \in [25, 100]$, with $\tilde{y} = 100$ is equivalent to a perfect health state ($y_a = 100\%, y_b = 0\%, y_c = 0\%, y_d = 0\%$), and $\tilde{y} = 25$ is equivalent the worst health state ($y_a = 0\%, y_b = 0\%, y_c = 0\%, y_d = 100\%$).

Furthermore, the interventions performed on structural elements are categorized according to their overall effect into, h_1: preventive maintenance, h_2: routine maintenance and h_3: repairs. These interventions are performed based on a recommendation from the inspector, and after violating a certain health condition threshold [24].

3.2 Missing Data and Outliers

Performing deterioration analysis on a large dataset of elements and structures requires handling missing data and outliers. This is done using different methods and criteria which are discussed in details in this section.

3.2.1 Missing Structural Attributes

Structural attributes represent distinctive information about each bridge, such as the annual average of daily traffic (AADT), the annual average of daily truck-traffic (AADTT), the bridge's age and the span length. In the context of this study, missing attributes can be either 1) missing covariates (i.e., traffic data), or 2) missing elements quantities. In the case of covariates, missing information are imputed using the k-nearest neighbour algorithm (k-NN) [14], where the missing covariate is estimated based on the data of $k = 5$ nearest bridges. On the other hand, if an element's quantity d_p^j is missing, the average quantity of elements within the same structural category is considered for replacing the missing value.

3.2.2 Missing Interventions

There are three possible scenarios for missing interventions, which are either, 1) the type of intervention h_r is missing, 2) the prior estimate for the effect of an intervention δ_r on structural category $\mathcal{S}_m^{j,*}$ is unavailable, or 3) the intervention is not reported in the database.

In the first scenario where the year of intervention τ is known and defined in the range ($t_0 < \tau < \mathtt{T}_p$), but the type of intervention h_r is missing, the type of h_r is determined using the maximum likelihood estimate (MLE), with the log-likelihood described by,

$$\mathcal{L}_h(h_r) = \sum_{t=t_0}^{\mathtt{T}_p} \ln f(y_{t,p}^j | y_{1:t-1,p}^j, h_r, \boldsymbol{\theta}), \tag{5}$$

where $\mathcal{L}_{h_r}$ is the log-likelihood estimate for applying the effect of intervention $\boldsymbol{\delta}_r$ associated with intervention type h_r, and t_0, $\mathtt{T}_p$ are the first and last timestamps with inspection data. For the second scenario where the year of intervention τ and the type of intervention h_r are known, but the effect of intervention $\boldsymbol{\delta}_r$ is not available, the average estimate of the same intervention type h_r in other structural categories $\mathcal{S}_{1:\mathtt{S}_*}^{j,*}$ is utilized in approximating the missing values.

The third scenario is when interventions on bridges are not reported in the database, which is common among small bridges, bridges with low traffic loads, and for certain types of structural elements. Figure 3 shows an example of a structural element which has an improvement in the condition with no records of interventions. From Figure 3, it is noticed that the condition has improved according to the observations, between years $t = 2011$ and $t = 2014$. This improvement is reported by the same inspector I_{12} who has reported the condition prior to the jump at the year $t = 2011$.

The presence of such cases can be handled using one of two options: the first option is to assume there was no intervention, which ultimately can result into a bias in the model estimates towards underestimating the condition, as shown in Figure 3. The second option is to examine the possibility of unreported intervention at the time of the positive jump in the condition. This can be done by verifying with the database if the bridge has underwent any type of maintenance on other structural elements at the same time of the positive jump. Detecting patterns of improvement in the inspection
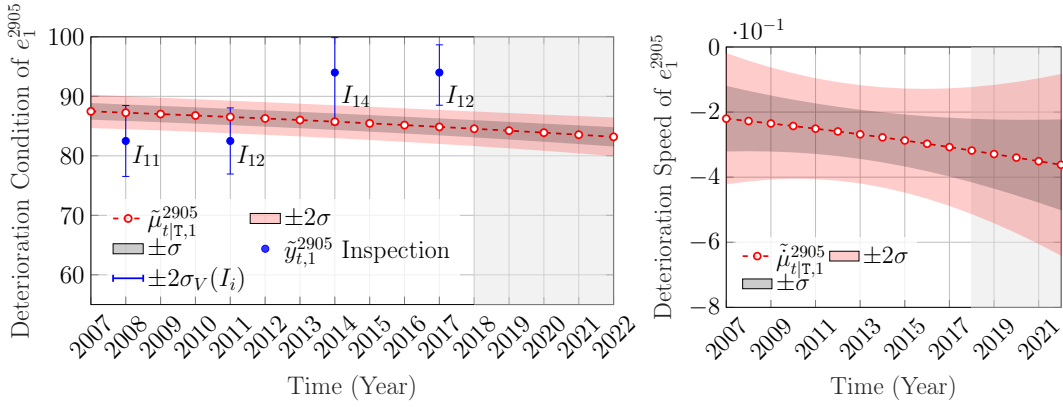
Figure 3: Deterioration state analysis for the condition and the speed based on the $\tilde{\boldsymbol{y}}_{t,1}^{2905} \in [25, 100]$ of *front-wall* element, error bars representing the inspectors' uncertainty estimates, and the shaded area representing the forecast period.

data of structural elements, can be done using the metric,

$$\Delta_p = \frac{\sum_t \Delta_{t,p}^+}{\sum_t |\Delta_{t,p}^\pm|}, \qquad \Delta_{t,p}^\pm = y_{t+\Delta t,p} - y_{t,p},$$

$$\Delta_{t,p}^+ = \begin{cases} \Delta_{t,p}^\pm, & \Delta_{t,p}^\pm > 0, \\ 0, & \Delta_{t,p}^\pm \le 0, \end{cases} \tag{6}$$

where Δ_p is the ratio between the total positive changes in the condition Δ_p^+, to all changes in the condition $\Delta_p^\pm$ for structural element e_p^j, with Δt being a reference to the time span between two consecutive observations. The ratio Δ_p is always positive and defined only for structural elements with three or more observations, and at least one observation showing improvement in the condition. Using the metric defined in Equation 6 on the same example in Figure 3, would yield $\Delta_1 = 1$. If an intervention is trigged for this case, the changes in the structural element's condition and speed now correspond to those shown in Figure 4.
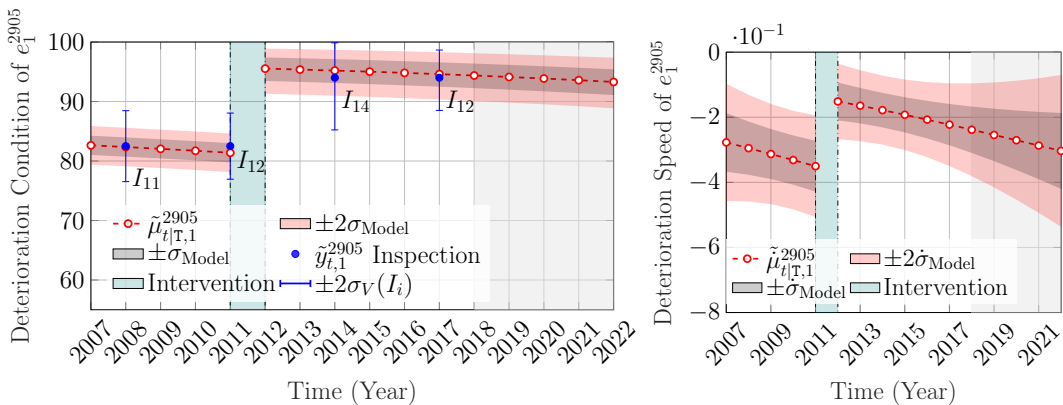

Figure 4: Deterioration state analysis for the condition and the speed based on the $\tilde{\boldsymbol{y}}_{t,1}^{2905} \in [25, 100]$ of *front-wall* element, with an intervention automatically triggered at $\tau = 2012$, error bars representing the inspectors' uncertainty estimates, and the shaded area representing the forecast period.

The network-scale analysis in this study are performed for both cases, i.e., using only the available intervention data, and accounting for the potentially unreported interventions through automatically triggering an intervention.

3.2.3 Handling Outliers

An outlier is a data point significantly different from other observations, which can have a negative effect on the model performance or can cause numerical instability in the update step of the Kalman filter (see Appendix A.1). The causes of an outlier are attributed either to 1) an incomplete interventions database, or 2) an erratic entry in the inspections database. In the context of visual inspections, an outlier is assumed to exist in the time-series if:

1. There is a significant difference between consecutive observations $\|y_{t+\Delta t,p} - y_{t,p}\| > 15$.

2. There is a significant condition improvement in a short period of time $\mathtt{T} < 8$ years, with observations, $\max(\boldsymbol{y}_{t,p}) - \min(\boldsymbol{y}_{t,p}) > 15$, and $\sum_{t=1}^{\mathtt{T}}(y_{t+\Delta t,p} - y_{t,p}) > 0$.

3. The number of observations indicating a significant improvement $y_{t+\Delta t} - y_t > 5$ in the structural element is greater than the number of observations indicating otherwise. Note that Δt refers to the time span between two consecutive observations.

If an outlier is detected based on the thresholds above, there are two possible lines of actions. If the outlier happened at a time t that matches the time τ of other interventions on the same bridge, then the outlier is classified as an intervention with the type h_r determined according to Equation 5. Otherwise, the outlier is considered as an erroneous inspection and is removed from the time-series. Removing an outlier is done by relying on the standard deviations $\sigma_V(I_i)$ associated with each inspection $y_{t,p}^j$. The timestamp associated with the outlier t_ϕ^j is determined based on the maximum difference between each inspection $y_{t,p}^j$, and the weighted average of all inspections $\hat{y}$, such that,

$$
\begin{aligned}
t_\phi^j &= \arg\max_t \|\boldsymbol{y}_{t,p}^j - \hat{y}\|, \\
\hat{y} &= \sum_t^{\mathtt{T}_p} y_{t,p}^j \frac{\phi_t}{\sum \phi_t},
\end{aligned}
\tag{7}
$$

where t_ϕ^j is the timestamp that corresponds to the outlier observation $y_{t_\phi,p}^j$, and $\hat{y}$ is a weighted average with the weights $\phi_t = \frac{1}{\sigma_V(I_i)}$. This approach allocates higher weights to more informative observations, which make inspections with a small $\sigma_V(I_i)$ unlikely to be selected for removal.

4 Case Studies

In this section, the capacity to aggregate the deterioration states is first demonstrated for individual bridges, followed by analyses on the entire network of bridges. It should be noted that for all examples, the model forecasts for years beyond the year 2020 are done while assuming that no interventions are performed.

4.1 Bridge without Interventions

The first case study is about the bridge $\mathcal{B}_{990}$, which is located in the Greater Montreal area. The length of the bridge is: $z_1 = 480.5$ m, which serves a traffic load AADT: $z_2 = 23700$, and AADTT: $z_3 = 1185$. The components that are visually inspected in the bridge are: $\mathtt{S}_1 = 8$ element categories from the primary elements group $\mathcal{G}_1^{990}$ and $\mathtt{S}_2 = 14$ element categories from the secondary elements group $\mathcal{G}_2^{990}$. Figure 5 shows a bar graph for the number of elements in each structural category. The top three categories with most structural elements in each structural group in bridge $\mathcal{B}_{990}$ are shown in Table 1, while the list of components is available in Appendix C.

The primary elements categories has a total of 143 elements, most of which are *beam* elements. Analyzing the deterioration of a structural category $\mathcal{S}_m^{j,*}$ for the bridge $\mathcal{B}_j$ requires modelling the deterioration for each element $e_p^j \in \mathcal{S}_m^{j,*}$. Thereafter, the overall deterioration state $\boldsymbol{s}_{t,m}^j$ of the structural category $\mathcal{S}_m^j$ can be obtained using the Gaussian mixture reduction approach described in Section 2.2, where the mixture weights are based on the element size d_p^j such that, $\lambda_p^j = \frac{d_p^j}{\sum_p d_p^j}$. An example that illustrates
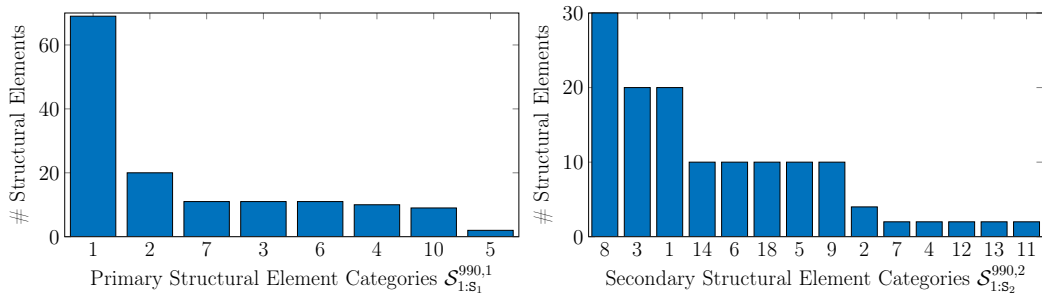
Figure 5: The number of elements within the primary and secondary structural element categories in bridge $\mathcal{B}_{990}$, with each category represented by a unique index defined in Tables C.3 and C.1.

Table 1: A subset of structural element categories sorted using descending order based on the number of elements in the bridge $\mathcal{B}_{990}$.

Primary $\mathcal{G}_1^{990}$	Secondary $\mathcal{G}_2^{990}$
$\mathcal{S}_1^{990,1}$: Beams	$\mathcal{S}_8^{990,2}$: Bracing
$\mathcal{S}_2^{990,1}$: External Sides	$\mathcal{S}_3^{990,2}$: Wheel Guard
$\mathcal{S}_7^{990,1}$: Bearing pad	$\mathcal{S}_1^{990,2}$: Safety Barriers (left or right)

the deterioration behaviour of a primary structural category is shown in Figure 6. In this figure, the overall deterioration condition $\tilde{s}_{t,m}^j$ and speed $\tilde{\dot{s}}_{t,m}^j$ are estimated for the *external-sides* element category $\mathcal{S}_2^{990,1}$, with $\tilde{y}_{op,t}^{990}$ representing the aggregated observations using the Gaussian mixture reduction for all $e_p^{990} \in \mathcal{S}_2^{990,1}$.
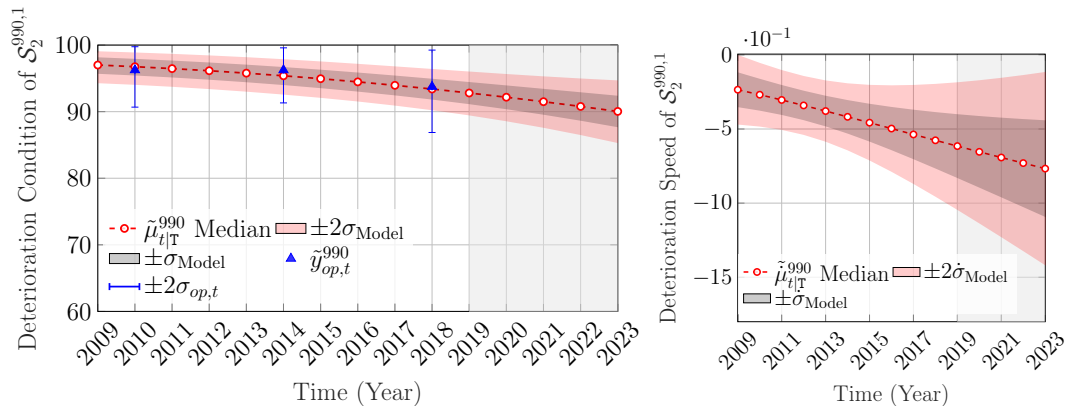

Figure 6: Deterioration state analysis for the condition and the speed based on the deterioration state estimates of *external-sides* elements $e_{1:20}^{990}$, with the aggregated observations $\tilde{y}_{op,t}^{990} \in [25, 100]$, and their corresponding uncertainty estimates represented by the error bars, with the shaded area representing the forecast period.

The overall deterioration state estimates $\tilde{g}_{t,1}^j$ for the primary structural group $\mathcal{G}_1^{990}$ is shown in Figure 7, which summarizes the deterioration state estimates for all primary structural elements in $\mathcal{B}_{990}$. These estimates are again obtained using the Gaussian mixture reduction approach, with the weights $\lambda_1^{990} = \frac{1}{s_1}$. Furthermore, $\tilde{y}_{gp,t}^{990}$ in Figure 7 represents the aggregation of all observations on the primary structural elements.

The deterioration analyses for a secondary structural category are demonstrated with an example case in Figure 8. This example illustrates the deterioration condition $\tilde{s}_{t,m}^{990,2}$ and speed $\tilde{\dot{s}}_{t,m}^{990,2}$ estimates for the *wheel guard* element category $\mathcal{S}_3^{990,2}$, with $\tilde{y}_{os,t}^{990}$ representing the aggregated observations in the secondary category $\mathcal{S}_3^{990,2}$. In Figure 8, the discrepancy between the model estimates and the aggregated observations is attributed to the initial deterioration speed, which is estimated based on
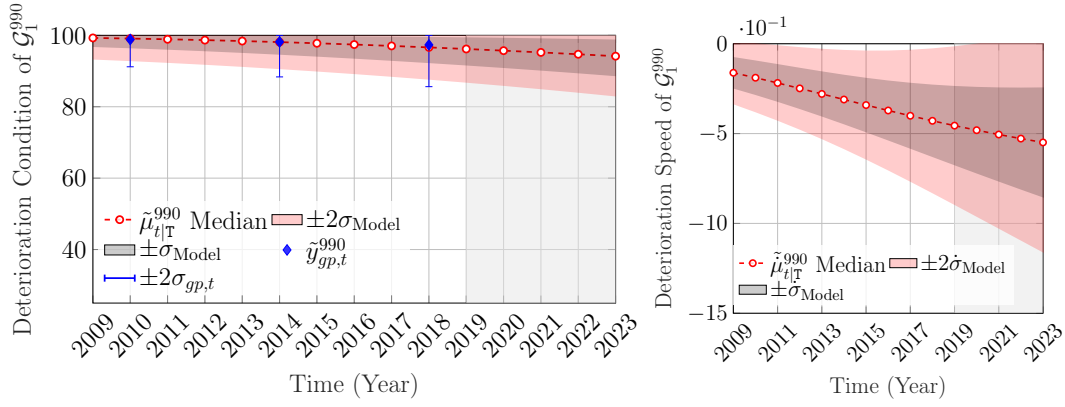
Figure 7: Deterioration state analysis for the condition and the speed of group $\mathcal{G}_1^{990}$, based on the deterioration state estimates of primary categories $\mathcal{S}_{1:\mathbf{s}_1}^{990,1}$, with the aggregated observations $\tilde{\boldsymbol{y}}_{gp,t}^{990} \in [25, 100]$, and their corresponding uncertainty estimates represented by the error bars, with the shaded area representing the forecast period.

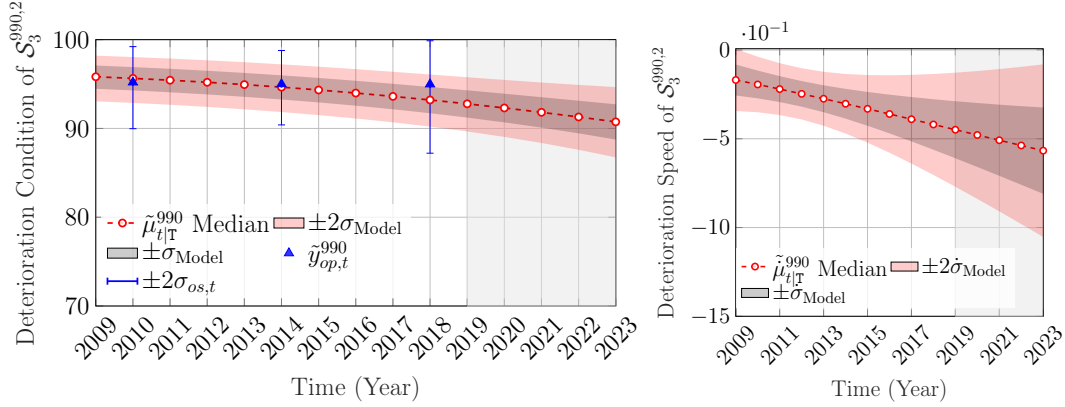the data from this bridge, as well as similar bridges that have *wheel guard* elements [12].

Figure 8: Deterioration state analysis for the condition and the speed based on the deterioration state estimates of *wheel guard* elements $e_{1:20}^{990}$, with the aggregated observations $\tilde{y}_{os,t}^{990} \in [25, 100]$, and their corresponding uncertainty estimates represented by the error bars, with the shaded area representing the forecast period.

The overall deterioration state estimates $\tilde{\boldsymbol{g}}_{t,2}^{990}$ for the secondary structural group $\mathcal{G}_2^{990} = \{\mathcal{S}_1^{990,2}, ..., \mathcal{S}_{\mathbf{s}_2}^{990,2}\}$ is shown in Figure 9. These estimates are obtained based on the deterioration condition $\tilde{s}_{t,1:\mathbf{s}_2}^{990,2}$ and speed $\tilde{\dot{s}}_{t,1:\mathbf{s}_2}^{990,2}$ estimates for each secondary category, and mixture weights $\lambda_2^j = \frac{1}{\mathbf{s}_2}$. From this figure, $\tilde{\boldsymbol{y}}_{gs,t}^{990}$ is the aggregated observation for the secondary structural group $\mathcal{G}_2^{990}$.

The results shown in this section demonstrate the capacity to aggregate the deterioration states of structural elements in order to obtain the overall deterioration state of the bridge, which is expressed by the deterioration state estimates for the primary $\mathcal{G}_1^j$, and the secondary $\mathcal{G}_2^j$ groups of structural elements.
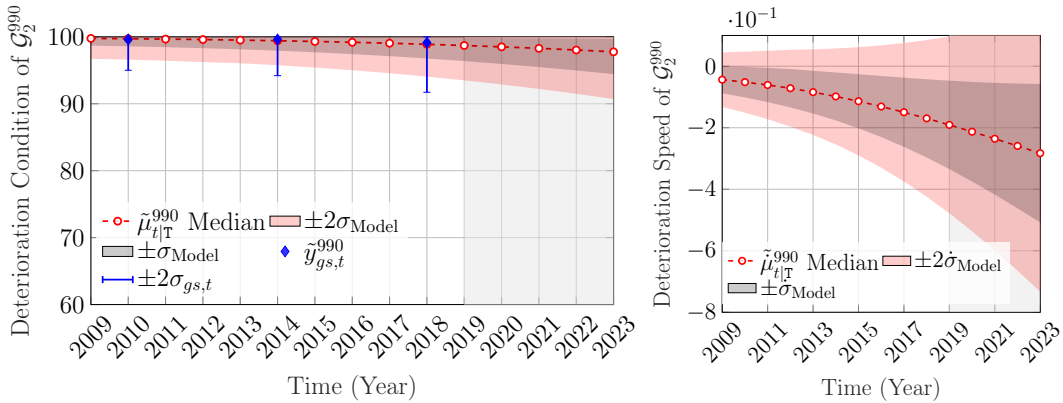
Figure 9: Deterioration state analysis for the condition and the speed of group $\mathcal{G}_2^{990}$, based on the deterioration state estimates of secondary categories $\mathcal{S}_{1:\mathbf{S}_2}^{990,2}$, with the aggregated observations $\tilde{\boldsymbol{y}}_{gs,t}^{990} \in [25,100]$, and their corresponding uncertainty estimates represented by the error bars, with the shaded area representing the forecast period.

4.2 Bridge with Interventions

In this case study, the deterioration analyses are performed for the visual inspection data for the bridge $\mathcal{B}_{3348}$, which is located in the Greater Montreal area, with a length: $z_1 = 64.5$ m, traffic load AADT: $z_2 = 53000$, and AADTT: $z_3 = 3710$. The interventions database indicates that the bridge has underwent repair works in year $\tau = 2015$, however, the annual costs database shows that the bridge have had also other interventions with unknown type earlier in the year $\tau = 2012$. The structural components that are visually inspected include $\mathbf{S}_1 = 8$ element categories from $\mathcal{G}_1^{3348}$, with 74 structural elements, and $\mathbf{S}_2 = 15$ element categories from $\mathcal{G}_2^{3348}$ with 54 structural elements. The bar graphs for $\mathcal{G}_1^{3348}$ and $\mathcal{G}_2^{3348}$ components are shown in Figure 10. In each graph, there are elements without interventions represented by the blue colour, elements with interventions represented by the red colour, and elements with uncategorized interventions represented by the orange colour. An uncategorized intervention is determined when the outlier criteria are met (see Section 3.2), and the outlier has occurred at a time t where interventions are reported in the database for the bridge on other structural elements.
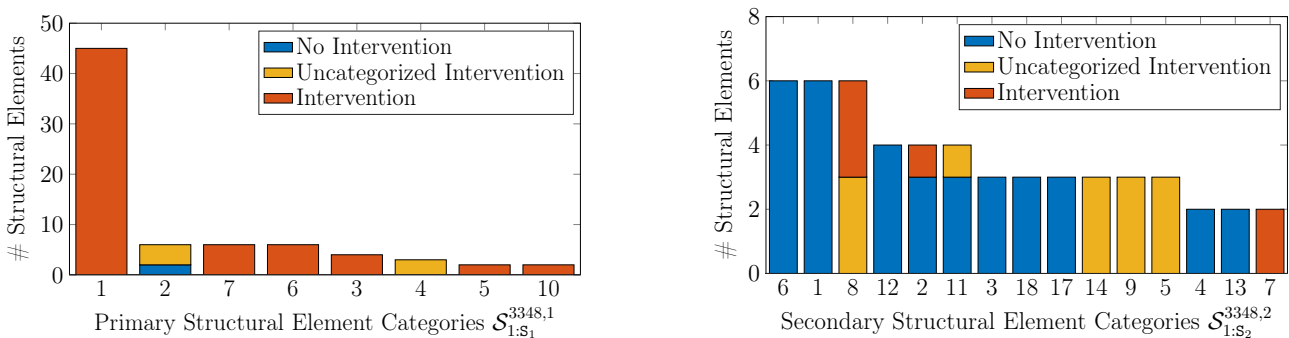

Figure 10: Primary and secondary structural element categories of bridge $\mathcal{B}_{3348}$ without interventions represented by the blue colour, with interventions represented by the red colour, and with uncategorized interventions in the orange.

The top three categories in each group are reported in Table 2, while the list of categories indexes is available in Tables C.3 and C.1. The deterioration analyses are performed on all the structural elements with visual inspection data using the SSM-KR deterioration model. An example for the deterioration analysis on a structural category $\mathcal{S}_m^{3348,1} \in \mathcal{G}_1^{3348}$ is shown in Figure 11. This example is for the deterioration analysis of the *slab* elements category $\mathcal{S}_4^{3348,1}$ based on inspection data from three *concrete slabs*. The state estimates for the deterioration condition $\tilde{s}_{t,4}^{3348,1}$ and speed $\tilde{\dot{s}}_{t,4}^{3348,1}$ are shown

Table 2: A subset of structural element categories sorted using descending order based on the number of elements in bridge $\mathcal{B}_{3348}$.

Primary $\mathcal{G}_1^{3348}$	Secondary $\mathcal{G}_2^{3348}$
$\mathcal{S}_1^{3348,1}$: Beams	$\mathcal{S}_6^{3348,2}$: Diaphragms
$\mathcal{S}_2^{3348,1}$: External Sides	$\mathcal{S}_1^{3348,2}$: Safety Barriers (left or right)
$\mathcal{S}_7^{3348,1}$: Bearing Pad	$\mathcal{S}_8^{3348,2}$: Bracing

in Figure 11. From this example, the aggregated observations $\tilde{\boldsymbol{y}}_{op,t}^{3348}$, and the model estimates $\tilde{\boldsymbol{s}}_{t,4}^{3348,1}$ after intervention are consistent with each other due to the small variability in the recorded data.
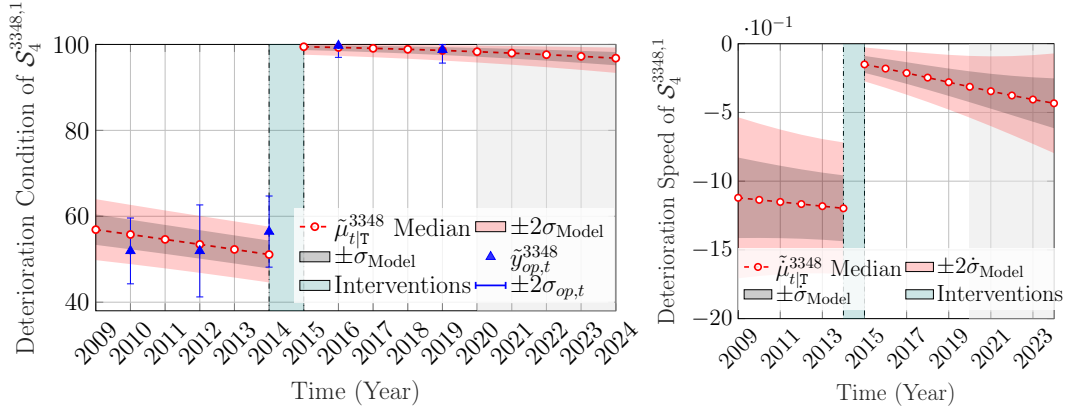

Figure 11: Deterioration state analysis for the condition and the speed based on the deterioration state estimates of *concrete slab* elements $e_{1:3}^{3348}$, with the interventions at time $\tau = 2015$, the aggregated observations $\tilde{\boldsymbol{y}}_{op,t}^{3348} \in [25, 100]$, with their corresponding uncertainty estimates represented by the error bars, and the shaded area representing the forecast period.

The overall state estimates for the primary structural group $\mathcal{G}_1^{3348}$ is shown in Figure 12. In Figure
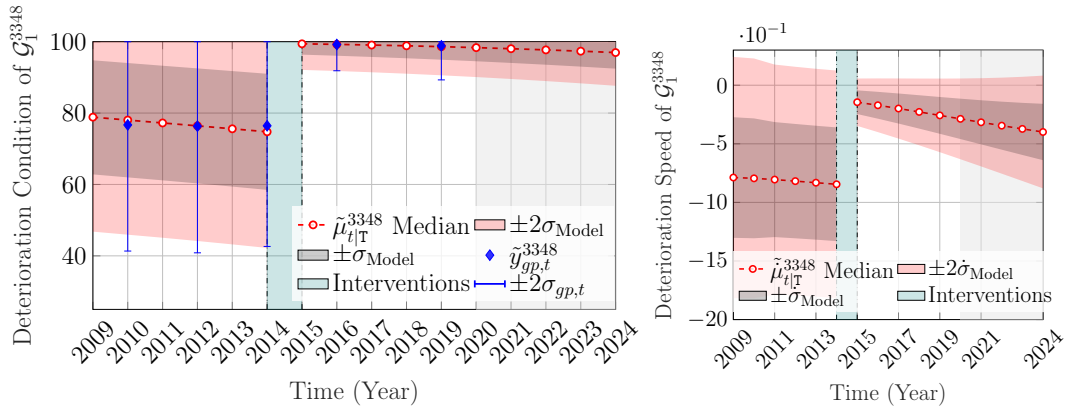

Figure 12: Deterioration state analysis for the condition and the speed based on the deterioration state estimates of the primary categories $\mathcal{S}_{1:\mathbf{s}_1}^{3348,1}$, with the interventions at time $\tau = 2015$, the aggregated observations $\tilde{\boldsymbol{y}}_{gp,t}^{3348} \in [25, 100]$, with their corresponding uncertainty estimates represented by the error bars, and the shaded area representing the forecast period.

12, the overall improvement due to interventions in the year $\tau = 2015$ is noticeable in the condition $\tilde{g}_{t,1}^{3348}$ and the speed $\tilde{\dot{g}}_{t,1}^{3348}$ state estimates. Moreover, the uncertainty of the state estimate prior to the intervention is significantly larger than the uncertainty after the intervention, which implies that there is a large variability between the elements' deterioration states before the interventions.

On the other hand, an example for the deterioration state estimates of $\mathcal{S}_m^{3348,2} \in \mathcal{G}_2^{3348}$, is shown in Figure 13. This example is for the *pavement* elements category $\mathcal{S}_5^{3348,2}$ which had an uncategorized

interventions in the year $\tau = 2015$. The type of intervention in this case is determined based on the MLE criterion described in Section 3.2.
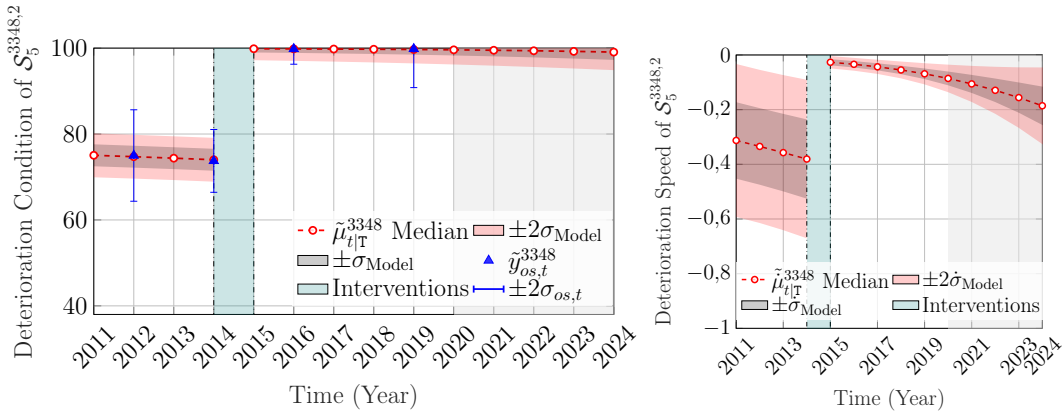

Figure 13: Deterioration state analysis for the condition and the speed based on the deterioration state estimates of *pavement* elements $e_{1:3}^{3348}$, with the interventions at time $\tau = 2015$, the aggregated observations $\tilde{\boldsymbol{y}}_{os,t}^{3348} \in [25, 100]$, with their corresponding uncertainty estimates represented by the error bars, and the shaded area representing the forecast period.

The overall deterioration state estimates $\tilde{\boldsymbol{g}}_{t,2}^{3348}$ for the secondary group $\mathcal{G}_2^{3348}$ are illustrated in Figure 14, which shows two major interventions at years $\tau_1 = 2012$ and $\tau_2 = 2015$. The first set of interventions
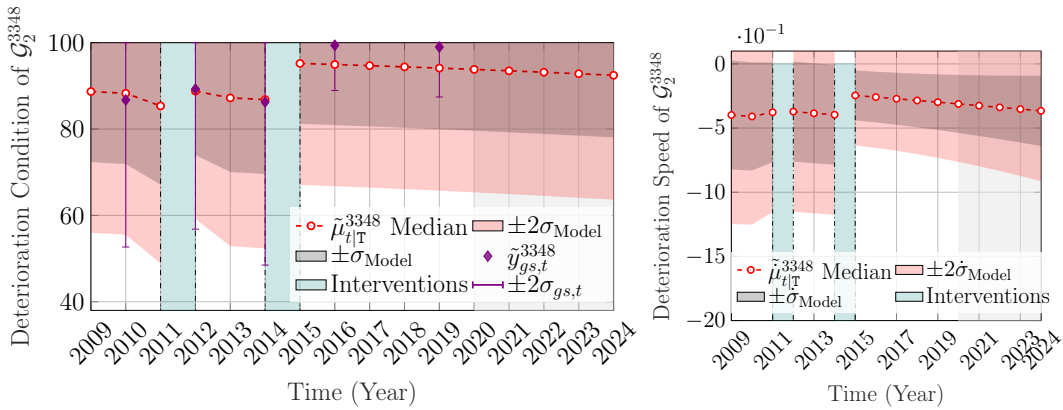

Figure 14: Deterioration state analysis for the condition and the speed based on the deterioration state estimates of the secondary categories $\mathcal{S}_{1:S_2}^{3348,2}$, with $\tilde{\boldsymbol{y}}_{gs,t}^{3348} \in [25, 100]$ representing the aggregation for a subset of observations, with their corresponding uncertainty estimates represented by the error bars, and the shaded area representing the forecast period.

is for the *sidewalk* elements category $\mathcal{S}_{11}^{3348,2}$, while the second set of interventions involved more elements categories, which overall resulted in significant improvement in $\mathcal{G}_2^{3348}$. Nonetheless, the uncertainty for $\mathcal{G}_2^{3348}$ is noticeably larger than the primary group $\mathcal{G}_1^{3348}$ in Figure 12. This is because there are two structural elements categories in $\mathcal{G}_2^{3348}$ that were not inspected in the year $t = 2015$ or afterwards, in addition to one element category is not inspected prior to year $t = 2015$, which led to $\tilde{\boldsymbol{y}}_{gs,t}^{3348}$ (distinguished with the violet colour) representing the aggregation for a subset of observations in $\mathcal{G}_2^{3348}$.

The results in this section have demonstrated the capacity to aggregate the deterioration states of elements with interventions, in order to obtain the overall deterioration states for the bridge $\mathcal{B}_{3348}$. It is noticeable in this case that the overall deterioration states for $\mathcal{G}_1^{3348}$ and $\mathcal{G}_2^{3348}$ have a higher uncertainty relative to the previous case in Section 4.1. This is attributed to the uncertainty associated with the effect of interventions, in addition to not performing post-intervention inspections for some of the structural elements.

4.3 Deterioration State of the Network

After estimating the deterioration state for each bridge $\mathcal{B}_j \in \mathcal{Q}$, it becomes feasible to estimate the overall deterioration state of the network for the primary structural elements group $\tilde{\boldsymbol{q}}_{t,1}$, and the secondary structural elements group $\tilde{\boldsymbol{q}}_{t,2}$. The main goals in this case study are,

1. Examine the overall network-scale deterioration state estimates over time.

2. Quantify the effect of interventions performed on the network throughout the time-window of inspections.

For that end, a network of bridges $\mathcal{Q}$ is considered, with $\mathtt{B} \approx 7000$ bridges located in the province of Quebec, Canada. The structural categories involved in the analyses are illustrated in Figure 15. The
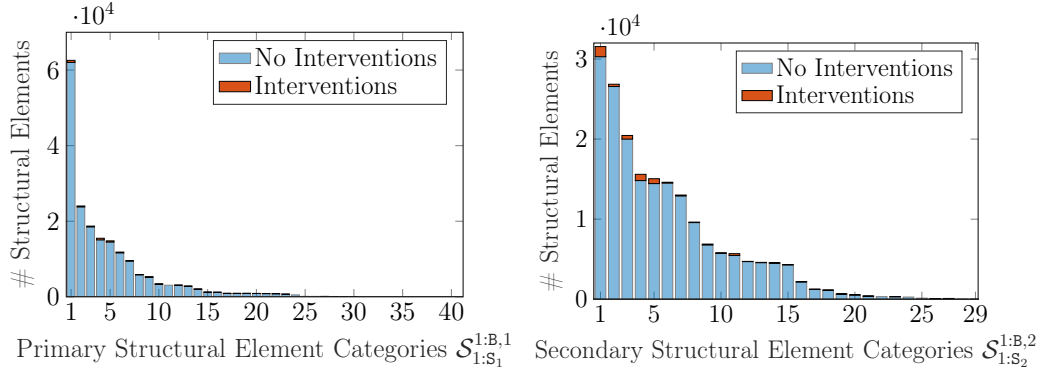

Figure 15: Primary $\mathcal{S}_{1:\mathtt{S}_1}$ and secondary $\mathcal{S}_{1:\mathtt{S}_1}$ structural elements categories without interventions represented by the light blue colour and with interventions represented by the red colour, with the categories sorted in a descending order based on the number of elements, and each category index defined in Tables C.3 and C.1.

top three categories in each group are reported in Table 3, while the full list of categories are reported in Appendix C. From the bar chart, it is noticed that there is a variability in the number of structural elements that belong to each structural category.

Table 3: A subset of structural element groups sorted using descending order based on the number of elements in each category.

Primary $\mathcal{G}_1^{1:\mathtt{B}}$	Secondary $\mathcal{G}_2^{1:\mathtt{B}}$
$\mathcal{S}_1$: Beams	$\mathcal{S}_1$: Safety Barriers (left or right)
$\mathcal{S}_2$: Bearing Seat	$\mathcal{S}_2$: Wing/Return Walls
$\mathcal{S}_3$: Bearing pad	$\mathcal{S}_3$: Wheel Guard

The inspections time-window for the set of bridges $\mathcal{Q}$ is from year $t = 2009$ to year $t = 2019$, during which multiple interventions are performed, that are further discussed in Section 4.4.

Estimating the deterioration state for the network is done based on the aggregation of the deterioration state estimates for all bridges using the GMR approach defined in Equation 3. From the preliminary analysis performed on bridges, it is concluded that there is no significant differences among the overall state estimates of the network's condition, when using weights based on factors such as the annual average of daily traffic (AADT) or bridge length (see Appendix B). Therefore, in this case study an equal weight $\lambda_j = \frac{1}{\mathtt{B}}$ is considered for all bridges when estimating the overall deterioration state of the network $\tilde{\boldsymbol{q}}_{t,1}$ and $\tilde{\boldsymbol{q}}_{t,2}$.

Figures 16 and 17 show the network's condition and speed estimates for the primary and secondary structural elements. From Figures 16 and 17, approximately 95% of bridges have a condition $\tilde{\mu}_{t|\mathtt{T}} \in [74, 100]$ for the primary structural elements, and $\tilde{\mu}_{t|\mathtt{T}} \in [71, 100]$ for the secondary structural elements, and overall, the health state for the secondary structural elements is higher than the primary structural elements. This is attributed to the frequency of interventions for the secondary structural elements
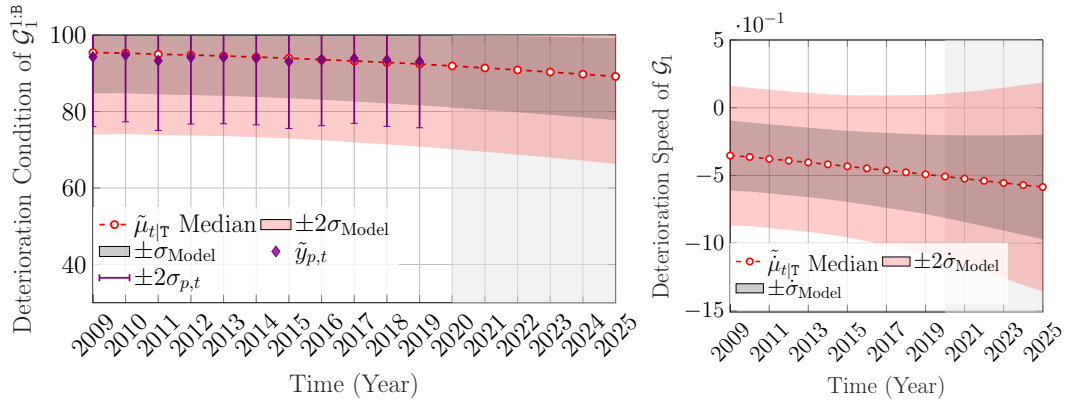
Figure 16: Deterioration state analysis for the network's condition and speed based on the average state of the primary structural elements from B ≈ 7000 bridges, with the shaded area representing the forecast period.

Figure 17: Deterioration state analysis for the network's condition and speed based on the average state of the secondary structural elements from B ≈ 7000 bridges, with the shaded area representing the forecast period.

being higher, relative to the primary structural elements (see Figure 20 in Section 4.4).

Nonetheless, the network's condition estimates in Figures 16 and 17, do not fully match the aggregated inspection data, especially in the case of the secondary group $\mathcal{G}_2^{1:B}$. This is attributed to the incompleteness of the database, and having unreported interventions as discussed in Section 3.2. In order to assess the effect of unreported interventions, the criterion defined in Equation 6 is applied to identify structural elements with improving patterns and automatically trigger an intervention event. In this case, an intervention is triggered automatically if more than 90% of the changes among the observations indicate improvement in the condition (i.e., $\Delta_p > 0.9$) for any structural element e_p^j. The deterioration state estimates of the modified framework are shown in Figures 18 and 19.

The modified framework shows an overall better association with the trend of the inspection data, compared to the original framework (Figures 16 and 17). Therefore, in the case relying only on the available interventions database, the network's condition and speed estimates presented in Figures 16 and 17, can be interpreted as lower bound estimates.

Furthermore, it should be taken into consideration that the estimates presented in this section are only based on the visually inspected elements, whereas it is possible to have some structural elements that are not included in the inspection process.

Figure 18: Deterioration state analysis for the network's condition and speed based on the average state of the primary structural elements from B ≈ 7000 bridges, with automatically triggered interventions, and the shaded area representing the forecast period.
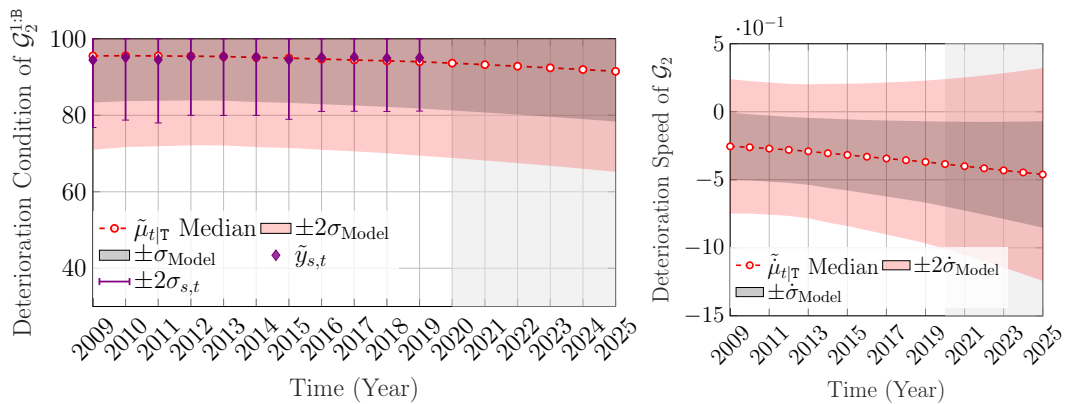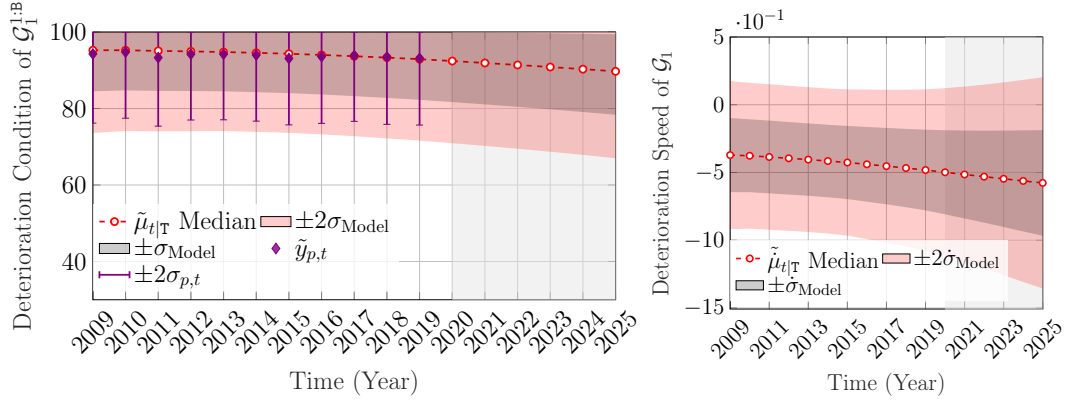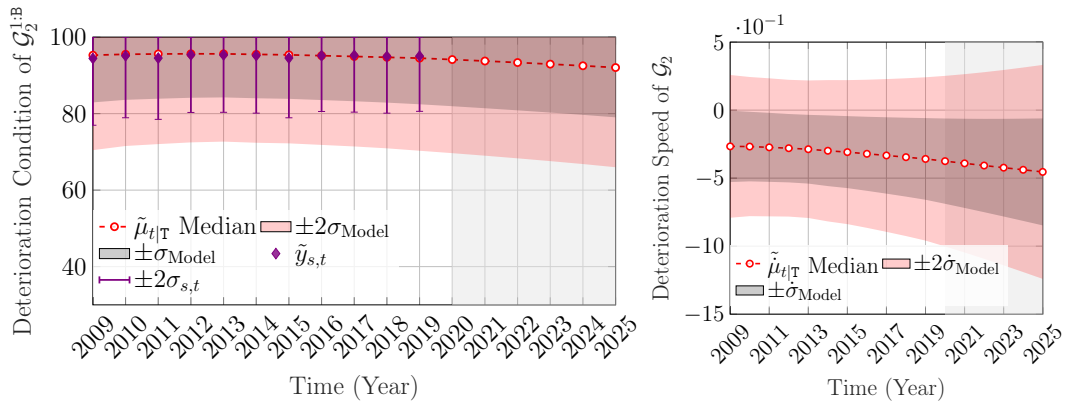

Figure 19: Deterioration state analysis for the network's condition and speed based on the average state of the secondary structural elements from B ≈ 7000 bridges, with automatically triggered interventions, and the shaded area representing the forecast period.

4.4 Network-Scale Effect of Interventions and Investments

The effects of interventions are quantified for each structural category $\mathcal{S}_m^{j,*}$ as part of the network-scale deterioration analysis. Figure 20 illustrates the cumulative ratio for the total number of elements with interventions $\mathtt{E}_r$ over the total number of inspected elements $\mathtt{E}$.
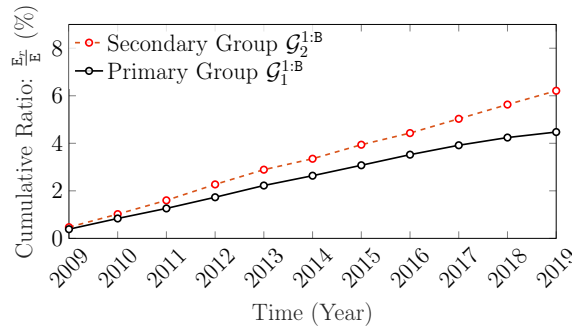
Figure 20: Cumulative ratio for the total number of elements with inspections $\mathtt{E}_r$ to the total number of visually inspected elements $\mathtt{E}$, in each structural group $\mathcal{G}_1^{1:\mathtt{B}}$ and $\mathcal{G}_2^{1:\mathtt{B}}$.

From Figure 20, it is noticed that since the year 2009 approximately 6% of the total number of inspected secondary elements have underwent interventions, compared to 4% of the primary elements.
The network-scale expected improvement in the condition for each structural category is reported

in Appendix C. These estimates are based on the framework presented in Hamida and Goulet[13], which relies on the intervention/inspection data available for each structural category $\mathcal{S}_m^{j,*}$. Based on the estimates in Appendix C, the overall aggregated expected improvement in the condition for the primary structural elements $\mathcal{G}_1^{1:B}$ and the secondary structural elements $\mathcal{G}_2^{1:B}$ are reported in Table 4.

Table 4: Aggregated expected improvement in the condition for the primary structural elements $\mathcal{G}_1^{1:B}$ and the secondary structural elements $\mathcal{G}_2^{1:B}$.

Structural Group	$\hat{\mu}_1^{\delta} \pm \hat{\sigma}_1^{\delta}$	$\hat{\mu}_2^{\delta} \pm \hat{\sigma}_2^{\delta}$	$\hat{\mu}_3^{\delta} \pm \hat{\sigma}_3^{\delta}$
Primary $\mathcal{G}_1^{1:B}$	0.8±5.5	10.7±8.3	14.7 ± 9.4
Secondary $\mathcal{G}_2^{1:B}$	17.5±3.8	9.5±6.5	17.9 ± 5.4

From Table 4, the aggregated improvements in the condition associated with the primary structural elements $\mathcal{G}_1^{1:B}$ coincides with the initial assumption that the h_1 type of interventions have a minor effect relative to h_2 and h_3. However, this is not the case for the secondary structural elements $\mathcal{G}_2^{1:B}$, as h_1 interventions show a significant effect on the condition. The reason behind this discrepancy is that minor interventions for the secondary structural elements are under-reported in the database (see Table C.3), and thus the estimated effect of h_1 is based only on two structural categories, of which in both of them, h_1 have a significant effect on the condition. An example for a reported h_1 intervention in the secondary elements $\mathcal{G}_2^{1:B}$, is the *asphalt resurfacing* for the *pavement* elements [24]. Note that Table 4 is provided to give an overview of the overall effect of interventions, but is not necessarily fully representative, as many types of interventions are under-reported (see Appendix C). In addition to the effect of intervention, the service-life for interventions on each category of element is presented in Tables C.2-C.4 of Appendix C. The service-life analysis represent the number of years before returning to the pre-intervention condition, which can be estimated using the approach described in Hamida and Goulet[13].

In order to assess the relation between interventions and costs, only bridges with reported costs are considered, where $\mathcal{Q}_c \subset \mathcal{Q}$ and $\mathtt{B}_c = 2999$ bridges. Figure 21 shows a comparisons between the costs, number of interventions and the network-scale expected improvement in the condition following an intervention. All values in this figure are aggregated for each year, and the relative values are considered in order to perform the comparisons. From Figure 21, it is noticed that the highest costs are associated with years 2009-2012, which also correspond to the highest network-scale expected improvement in the condition, and some of the highest number of interventions performed. Nonetheless, intervention costs can vary among the structural categories, as well as the type of interventions performed, therefore, it is not a necessity for the number of interventions to be perfectly correlated with the costs.

(a) Relative aggregated costs vs. the relative aggregated number of interventions

(b) Relative aggregated costs vs. the relative network-scale expected condition improvement
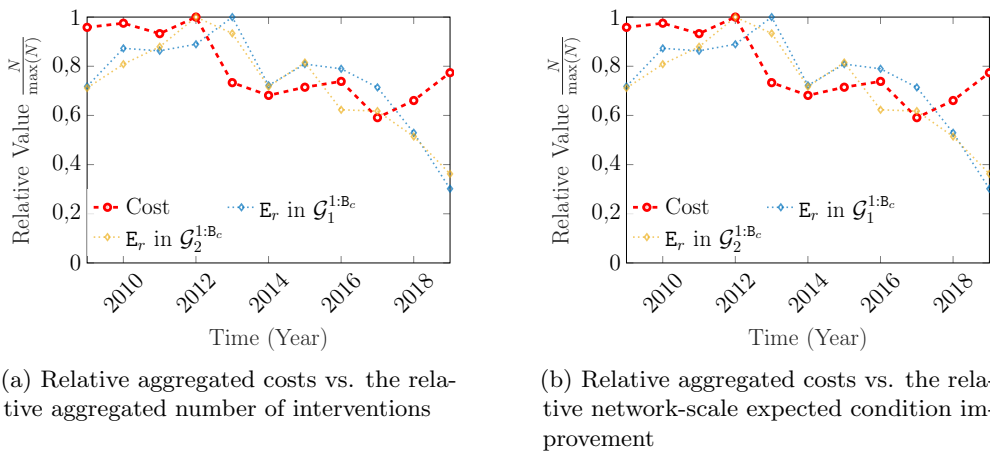
Figure 21: Comparison between the costs, number of interventions $\mathtt{E}_r$, and the network-scale expected condition improvement $\mathbb{E}[\mu^{\delta}]$ for interventions performed on the primary and secondary structural elements from $\mathtt{B}_c = 2999$ bridges.

5 Conclusion

In this study, the application of SSM/SSM-KR deterioration model is extended beyond structural elements to include estimates for the deterioration state of structural systems, bridges, as well as the entire network. The hierarchy of systems in any bridge $\mathcal{B}_j$ consists of two groups at the top, primary $\mathcal{G}_1^j$, and secondary $\mathcal{G}_2^j$, with each group encompassing multiple structural categories $\mathcal{S}_m^{j,*}$, and each structural category containing a number of structural elements e_p^j. Estimating the deterioration state for a structural category $\mathcal{S}_m^{j,*}$ is done based on the deterioration state estimates of the structural elements within it, and by using a Gaussian mixture reduction approach with the weights determined based on the quantity associated with each element $e_p^j \in \mathcal{S}_m^{j,*}$. Following the estimation for the deterioration states of all categories within a bridge, the deterioration states $\tilde{\boldsymbol{g}}_{t,*}^j$ for the structural group $\mathcal{G}_*^j$ are estimated using equal aggregation weights. These analyses are followed by assessing the network's deterioration state $\tilde{\boldsymbol{q}}_t$ based on $\texttt{B} \approx 7000$ bridges, and by using equal aggregation weights for all bridges. From the analysis, it is found that approximately 95% of bridges have a condition $\tilde{\mu}_{t|\texttt{T}} \in [74, 100]$ for $\mathcal{G}_1^{1:\texttt{B}}$, and $\tilde{\mu}_{t|\texttt{T}} \in [71, 100]$ for $\mathcal{G}_2^{1:\texttt{B}}$, and overall, the health state is sustained at a high level. Finally, the spending costs associated with interventions are analyzed for a subset of bridges. The analysis involves a comparison between the costs, the improvement in the health state, and the number of interventions. The comparison results have shown that the highest investments were associated with the highest expected improvements in the network's condition but not necessarily the highest number of interventions at a given year. Such a discrepancy is justified because intervention costs can vary among the structural categories, as well as the type of interventions performed. Overall, the methods presented in this work demonstrated the capacity to quantify the deterioration states of bridges based on visual inspections, which lays the foundation for network-scale planning of maintenance activities.

Acknowledgements

A SSM-based Deterioration Model

A.1 Kalman Filter and Kalman Smoother Formulation

The Kalman filter (KF) describes the transition from the hidden state $\boldsymbol{x}_{t-1}$ to the hidden state $\boldsymbol{x}_t$ based on two steps, the prediction step and the update step. The prediction step is expressed by,

$$E[\boldsymbol{X}_t|\boldsymbol{y}_{1:t-1}] \equiv \boldsymbol{\mu}_{t|t-1} = \boldsymbol{A}_t \boldsymbol{\mu}_{t-1|t-1}$$
$$\text{cov}[\boldsymbol{X}_t|\boldsymbol{y}_{1:t-1}] \equiv \boldsymbol{\Sigma}_{t|t-1} = \boldsymbol{A}_t \boldsymbol{\Sigma}_{t-1|t-1} \boldsymbol{A}^\intercal + \boldsymbol{Q}_t,$$

where $E[\boldsymbol{X}_t|\boldsymbol{y}_{1:t-1}]$ and $\text{cov}[\boldsymbol{X}_t|\boldsymbol{y}_{1:t-1}]$ represent the expected value and covariance of the hidden state vector $\boldsymbol{x}_t$ at time t given all the observations $\boldsymbol{y}_{1:t-1}$ up to time $t-1$, $\boldsymbol{A}_t$ is the transition matrix and $\boldsymbol{Q}_t$ is the model error covariance matrix. In the context of this study, the transition matrix $\boldsymbol{A}_t$ is defined by,

$$\boldsymbol{A}_{t=\tau} = \left[\begin{array}{cc} \boldsymbol{A}^{\texttt{ki}} & \boldsymbol{I}_{3\times 3} \\ \boldsymbol{0}_{3\times 3} & \boldsymbol{I}_{3\times 3} \end{array} \right], \ \boldsymbol{A}_{t\neq\tau} = \left[\begin{array}{cc} \boldsymbol{A}^{\texttt{ki}} & \boldsymbol{0}_{3\times 3} \\ \boldsymbol{0}_{3\times 3} & \boldsymbol{I}_{3\times 3} \end{array} \right], \ \boldsymbol{A}^{\texttt{ki}} = \left[\begin{array}{ccc} 1 & dt & \frac{dt^2}{2} \\ 0 & 1 & dt \\ 0 & 0 & 1 \end{array} \right],$$

where $\boldsymbol{I}$ is the identity matrix and τ represents the time of intervention. The matrix $\boldsymbol{Q}_t$ is defined as in,

$$\boldsymbol{Q}_{t=\tau} = \left[\begin{array}{cc} \boldsymbol{Q}^{\texttt{ki}} + \boldsymbol{Q}^r & \boldsymbol{0}_{3\times 3} \\ \boldsymbol{0}_{3\times 3} & \boldsymbol{Q}^r \end{array} \right], \ \boldsymbol{Q}_{t\neq\tau} = \left[\begin{array}{cc} \boldsymbol{Q}^{\texttt{ki}} & \boldsymbol{0}_{3\times 3} \\ \boldsymbol{0}_{3\times 3} & \boldsymbol{0}_{3\times 3} \end{array} \right],$$

with $\boldsymbol{Q}^r$ and $\boldsymbol{Q}^{\texttt{ki}}$ defined as,

$$\boldsymbol{Q}^r = \text{diag}\left(\left[\sigma_{w_r}^2 \; \dot{\sigma}_{w_r}^2 \; \ddot{\sigma}_{w_r}^2\right]\right), \; \boldsymbol{Q}^{\texttt{ki}} = \sigma_w^2 \begin{bmatrix} \frac{dt^5}{20} & \frac{dt^4}{8} & \frac{dt^3}{6} \\ \frac{dt^4}{8} & \frac{dt^3}{3} & \frac{dt^2}{2} \\ \frac{dt^3}{6} & \frac{dt^2}{2} & dt \end{bmatrix},$$

where dt is the time step size, σ_w is a model parameter that describe the kinematic model process noise and $\boldsymbol{Q}^r$ is a diagonal matrix that conttain model parameters describing the element-level intervention errors [13]. Following the prediction step, if an observation is available at time t, the expected value and covariance estimates are updated with the observation information using the update step,

$$f(\boldsymbol{x}_t|\boldsymbol{y}_{1:t}) = \mathcal{N}(\boldsymbol{x}_t; \boldsymbol{\mu}_{t|t}, \boldsymbol{\Sigma}_{t|t})$$
$$\boldsymbol{\mu}_{t|t} = \boldsymbol{\mu}_{t|t-1} + \boldsymbol{K}_t(\boldsymbol{y}_t - \boldsymbol{C}\boldsymbol{\mu}_{t|t-1})$$
$$\boldsymbol{\Sigma}_{t|t} = (\boldsymbol{I} - \boldsymbol{K}_t\boldsymbol{C})\boldsymbol{\Sigma}_{t-1|t-1}$$
$$\boldsymbol{K}_t = \boldsymbol{\Sigma}_{t-1|t-1}\boldsymbol{C}^\intercal \boldsymbol{G}_t^{-1}$$
$$\boldsymbol{G}_t = \boldsymbol{C}\boldsymbol{\Sigma}_{t-1|t-1}\boldsymbol{C}^\intercal + \boldsymbol{R}_t,$$

where $\boldsymbol{\mu}_{t|t} \equiv E[\boldsymbol{X}_t|\boldsymbol{y}_{1:t}]$ and $\boldsymbol{\Sigma}_{t|t} \equiv \text{cov}[\boldsymbol{X}_t|\boldsymbol{y}_{1:t}]$ are the posterior expected value and covariance at time t, conditional to the observations up to time t, $\boldsymbol{I}$ is the identity matrix, $\boldsymbol{K}_t$ is the Kalman gain, and $\boldsymbol{G}_t$ is the innovation covariance. On the other hand, the RTS Kalman smoother (KS) [26] is a backward framework which relies on the information acquired after passing on all of the observations up to time $t = \texttt{T}$, to update each of the previous hidden states. The KS is described by the equations,

$$f(\boldsymbol{x}_t|\boldsymbol{y}_{1:\texttt{T}}) = \mathcal{N}(\boldsymbol{x}_t; \boldsymbol{\mu}_{t|T}, \boldsymbol{\Sigma}_{t|T})$$
$$\boldsymbol{\mu}_{t|\texttt{T}} = \boldsymbol{\mu}_{t|t} + \boldsymbol{J}_t(\boldsymbol{\mu}_{t+1|\texttt{T}} - \boldsymbol{\mu}_{t+1|t})$$
$$\boldsymbol{\Sigma}_{t|\texttt{T}} = \boldsymbol{\Sigma}_{t|t} + \boldsymbol{J}_t(\boldsymbol{\Sigma}_{t+1|\texttt{T}} - \boldsymbol{\Sigma}_{t+1|t})\boldsymbol{J}_t^\intercal$$
$$\boldsymbol{J}_t = \boldsymbol{\Sigma}_{t|t}\boldsymbol{A}^\intercal \boldsymbol{\Sigma}_{t+1|t}^{-1}.$$

In order to ensure the monotonicity throughout the estimation process, the deterioration speed constraints: $\dot{\mu}_{t|t} + 2\sigma_{t|t}^{\dot{x}} \leq 0$, are examined at each time step t, and enacted (if needed) using the PDF truncation method [29, 11].

A.2 Space Transformation & Transformation Function

Space transformation is performed using the transformation functions $o(\tilde{x})$ and $o^{-1}(x)$ [11]. The transformation function $o^{-1}(x)$ maps a deterioration state $x \in [-\infty, \infty]$, labelled as the unbounded space to $\tilde{x} \in [l, u]$, labelled as the bounded space. On the other hand the transformation function $o(\tilde{x})$ maps a deterioration state from the bounded space $\tilde{x} \in [l, u]$ to the unbounded space $x \in [-\infty, \infty]$. Each of the aforementioned functions are described by the equations below,

$$x = o(\tilde{x}) = \begin{cases} \left[\frac{1}{\Gamma(\alpha)}\int_0^{\tilde{x}} t^{\alpha-1}e^{-t}dt\right]^\alpha, & \frac{u+l}{2} < \tilde{x} \leq u, \\ \tilde{x}, & \tilde{x} = \frac{u+l}{2}, \\ -\left[\frac{1}{\Gamma(\alpha)}\int_0^{\tilde{x}} t^{\alpha-1}e^{-t}dt\right]^\alpha, & l \leq \tilde{x} < \frac{u+l}{2}, \end{cases} \qquad \tilde{x} = o^{-1}(x) = \begin{cases} \frac{1}{\Gamma(\alpha)}\int_0^{x^{\frac{1}{\alpha}}} t^{\alpha-1}e^{-t}dt, & x > \frac{u+l}{2}, \\ x, & x = \frac{u+l}{2}, \\ -\frac{1}{\Gamma(\alpha)}\int_0^{x^{\frac{1}{\alpha}}} t^{\alpha-1}e^{-t}dt, & x < \frac{u+l}{2}. \end{cases}$$

The parameter α in the equations above is given by: $\alpha = 2^{-n}$, where n is a positive integer $n \in \mathbb{Z}^+$. Further details about the estimation of n and its role are available in Hamida and Goulet [11].

B Network-Scale Deterioration Analysis Based on Bridges' Attributes

Figure B.1 shows scatter plots for bridges attributes, which are generated from $\texttt{B} \approx 7000$ bridges. From Figure B.1, it is noticed that AADTT has some correlation with AADT, demonstrated by similar peaks on the diagonal, while there is a little to no correlation between the traffic load and the bridge
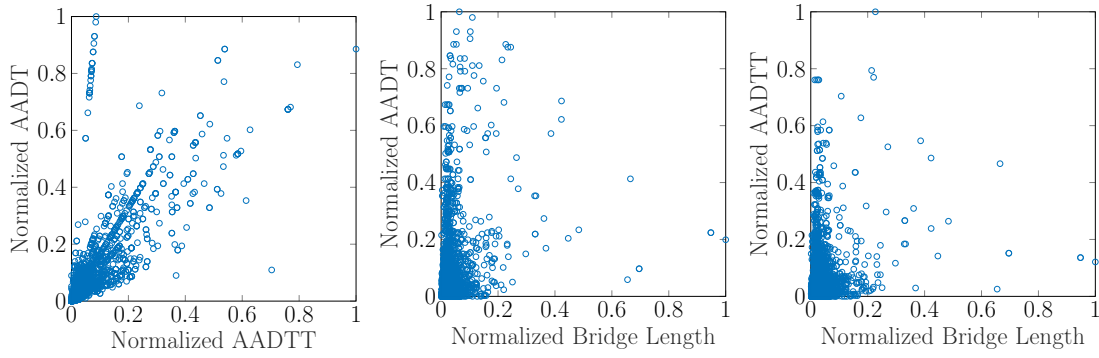
Figure B.1: Scatter plots for the normalized annual average of daily traffic (AADT) vs. the normalized annual average of daily truck-traffic (AADTT) vs. and the normalized length associated with each bridge in the network.

length. This assessment implies that the above mentioned factors are different from each other, and therefore each of them can be utilized to draw different conclusions about the overall state of the network.

Estimating the deterioration states for a network of bridges can be done using different approaches, one such approach is by taking the overall average for the deterioration states of all bridges in the network. However, such an approach assumes that the contribution of all bridges is equal across the network, which is a claim that requires validation; provided the large discrepancies in AADT and other attributes across the network [6]. Therefore, a weighted average, that relies on the available attributes, is considered in examining the overall deterioration condition and speed based on $B \approx 7000$ bridges. The weighted averages for each metric are estimated using the GMR approach defined in Equation 3. The estimation results are shown in Figure B.2, which outline the network's expected condition and speed in years 2020 and 2025, under the scenario that no maintenance interventions are performed. The letters in the acronyms on each axes are, P: primary, S: secondary, A: AADT, L: bridge length, M: number of bridges, T: AADTT. For example, in the network condition graph, PL refers to the (P)rimary condition of the network based on a weighted average, with the weights determined according to the bridge (L)ength (i.e., $\lambda^j = \frac{z_1^j}{\sum z_1}$).
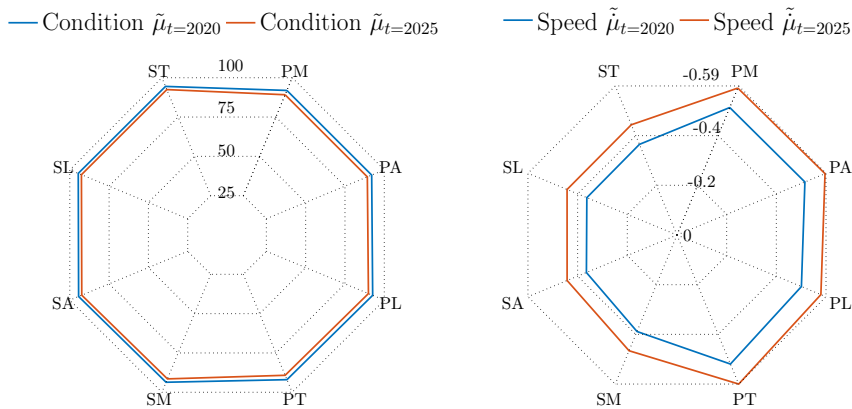
Figure B.2: Expected values for the network's deterioration condition and speed based on a weighted average of $B \approx 7000$ according to: number of bridges, AADT, bridge length and number of trucks for the primary and secondary groups.

Although the condition estimates in Figure B.2 show no apparent difference, the network's condition estimates weighted by the bridge length have the highest scores with, PL: $\tilde{\mu}_{t=2020} = 92.6 \in [25, 100]$, and SL: $\tilde{\mu}_{t=2020} = 94.6 \in [25, 100]$, compared to the weighted average based on the number of bridges, which has the lowest scores, PM: $\tilde{\mu}_{t=2020} = 91.91 \in [25, 100]$. On the other hand, the network's highest deterioration speed is associated with the estimates weighted by AADTT (i.e. $\lambda^j = \frac{z_3}{\sum z_3}$)

with, PT: $\tilde{\mu}_{t=2020} = -0.51$, for the primary group, while for the secondary group $\mathcal{G}_2$, the network's highest deterioration speed is associated with the estimates weighted by the number of bridges, SM: $\tilde{\mu}_{t=2020} = -0.38$. Moreover, it is noticed that there is a difference in the networks's deterioration speed between the primary and secondary groups. This is explained by the overall health condition of $\mathcal{G}_2^{1:B}$ being higher than the overall health condition of $\mathcal{G}_1^{1:B}$, which is also reflected by the number of interventions performed on the secondary group $\mathcal{G}_2$ compared to the primary group $\mathcal{G}_1^{1:B}$ (see Figure 20).

C Effect of Interventions on Structural Categories

Table C.1: Effect of interventions on the primary categories of structural elements.

Structural Category $\mathcal{S}_m^{1:B,1}$	$\mu_1^\delta \pm \sigma_1^\delta$	$\mu_2^\delta \pm \sigma_2^\delta$	$\mu_3^\delta \pm \sigma_3^\delta$	E_r
$\mathcal{S}_1$: Poutre	NA	NA	12.6 ± 0.8	548
$\mathcal{S}_2$: Côté extérieur	0.02 ± 1.2	NA	15.9 ± 1.2	248
$\mathcal{S}_3$: Assise	NA	NA	21.3 ± 1.8	213
$\mathcal{S}_4$: Platelage	1.9 ± 3.3	11.4 ± 2.2	20.6 ± 1.3	295
$\mathcal{S}_5$: Mur de front	NA	13.6 ± 1.4	17.6 ± 1.3	319
$\mathcal{S}_6$: Appareils d'appui	NA	NA	32.1 ± 1.6	221
$\mathcal{S}_7$: Blocs d'assise	NA	NA	27.5 ± 2.8	48
$\mathcal{S}_8$: Chevêtre	NA	NA	16.2 ± 2.1	77
$\mathcal{S}_9$: Colonnes / bancs	NA	NA	11.6 ± 0.8	165
$\mathcal{S}_{10}$: Fût	0.4 ± 1.1	7.1 ± 7.2	20.5 ± 2.1	86
$\mathcal{S}_{13}$: Radier	NA	NA	18.3 ± 2.8	11
$\mathcal{S}_{15}$: Entretoises	NA	NA	7.3 ± 7	9
$\mathcal{S}_{16}$: Colonnes	NA	NA	8.3 ± 0.8	5
$\mathcal{S}_{17}$: Montants / poteaux	NA	NA	NA	6
$\mathcal{S}_{18}$: Corde supérieure	NA	NA	NA	2
$\mathcal{S}_{19}$: Diagonales	NA	NA	2.3 ± 4.4	9
$\mathcal{S}_{20}$: Corde inférieure	NA	NA	7.9 ± 7.3	20
$\mathcal{S}_{21}$: Longerons	NA	NA	8.4 ± 7.1	9
$\mathcal{S}_{22}$: Assemblages	NA	NA	NA	5
$\mathcal{S}_{23}$: Diaphrag. extrém. int. ptres caissons	NA	NA	NA	1
$\mathcal{S}_{25}$: Corbeaux	NA	NA	NA	0
$\mathcal{S}_{26}$: Suspentes/montants	NA	NA	NA	0
$\mathcal{S}_{27}$: Tympan	NA	NA	NA	4
$\mathcal{S}_{28}$: Arc	NA	NA	13.6 ± 1.7	2
$\mathcal{S}_{29}$: Tirants	NA	NA	NA	5
$\mathcal{S}_{30}$: Voûte	NA	NA	2.8 ± 3.9	2
$\mathcal{S}_{31}$: Tirant	NA	NA	NA	0
$\mathcal{S}_{33}$: Bras d'articulation	NA	NA	NA	0
$\mathcal{S}_{34}$: Haubans et accessoires	NA	NA	NA	0
$\mathcal{S}_{35}$: Sabots d'attache des torons	NA	NA	NA	0
$\mathcal{S}_{36}$: Câble porteur et accessoires	NA	NA	NA	0
$\mathcal{S}_{37}$: Membrure supérieure	NA	NA	NA	0
$\mathcal{S}_{38}$: Suspentes et accessoires	NA	NA	NA	0
$\mathcal{S}_{39}$: Chambre d'épanouiss. câbles	NA	NA	NA	0
$\mathcal{S}_{40}$: Stabilisateurs transversaux	NA	NA	NA	0

NA: The results are not available due to limitations in the database.

Table C.2: Service-life (in years) before reaching the pre-intervention condition for the primary categories of structural elements having underwent interventions h_3, with the maximum forecast period fixed at 120 years.

Structural Category $\mathcal{S}_m^{1:\mathrm{B},1}$	10th percentile	50th percentile	90th percentile
$\mathcal{S}_1$: Poutre	6	18	33
$\mathcal{S}_2$: Côté extérieur	6	15	35
$\mathcal{S}_3$: Assise	6	24	70
$\mathcal{S}_4$: Platelage	5	12	26
$\mathcal{S}_5$: Mur de front	6	19	41
$\mathcal{S}_6$: Appareils d'appui	6	42	66
$\mathcal{S}_7$: Blocs d'assise	15	34	63
$\mathcal{S}_8$: Chevêtre	10	29	50
$\mathcal{S}_9$: Colonnes / bancs	6	16	33
$\mathcal{S}_{10}$: Fût	4	13	27
$\mathcal{S}_{13}$: Radier	22	30	40
$\mathcal{S}_{15}$: Entretoises	4	12	44
$\mathcal{S}_{16}$: Colonnes	10	14	18
$\mathcal{S}_{17}$: Montants / poteaux	NA	NA	NA
$\mathcal{S}_{18}$: Corde supérieure	NA	NA	NA
$\mathcal{S}_{19}$: Diagonales	NA	NA	NA
$\mathcal{S}_{20}$: Corde inférieure	NA	NA	NA
$\mathcal{S}_{21}$: Longerons	6	11	31
$\mathcal{S}_{22}$: Assemblages	NA	NA	NA
$\mathcal{S}_{23}$: Diaphrag. extrém. int. poutres caissons	NA	NA	NA
$\mathcal{S}_{25}$: Corbeaux	NA	NA	NA
$\mathcal{S}_{26}$: Suspentes/montants	NA	NA	NA
$\mathcal{S}_{27}$: Tympan	NA	NA	NA
$\mathcal{S}_{28}$: Arc	14	19	28
$\mathcal{S}_{29}$: Tirants	9	24	38
$\mathcal{S}_{30}$: Voûte	13	15	19
$\mathcal{S}_{31}$: Tirant	NA	NA	NA
$\mathcal{S}_{33}$: Bras d'articulation	NA	NA	NA
$\mathcal{S}_{34}$: Haubans et accessoires	NA	NA	NA
$\mathcal{S}_{35}$: Sabots d'attache des torons	NA	NA	NA
$\mathcal{S}_{36}$: Câble porteur et accessoires	NA	NA	NA
$\mathcal{S}_{37}$: Membrure supérieure	NA	NA	NA
$\mathcal{S}_{38}$: Suspentes et accessoires	NA	NA	NA
$\mathcal{S}_{39}$: Chambre d'épanouiss. câbles	NA	NA	NA
$\mathcal{S}_{40}$: Stabilisateurs transversaux	NA	NA	NA

NA: The results are not available due to limitations in the database.

Table C.3: Effect of interventions on the secondary categories of structural elements.

Structural Category $\mathcal{S}_m^{1:B,2}$	$\mu_1^\delta \pm \sigma_1^\delta$	$\mu_2^\delta \pm \sigma_2^\delta$	$\mu_3^\delta \pm \sigma_3^\delta$	E_r
$\mathcal{S}_1$: Glissière (gauche ou droite)	NA	NA	20.6 ± 1.4	1269
$\mathcal{S}_2$: Murs en aile / en retour	NA	NA	18 ± 1.3	285
$\mathcal{S}_3$: Chasse-roue	NA	NA	18.3 ± 1.4	455
$\mathcal{S}_4$: Glissière	NA	9.3 ± 3	15.4 ± 0.8	782
$\mathcal{S}_5$: Surface de roulement	20.9 ± 2	NA	27.7 ± 1.2	610
$\mathcal{S}_6$: Diaphragmes	NA	NA	16.9 ± 3.1	107
$\mathcal{S}_7$: Garde-grève	NA	7.8 ± 7.3	21.8 ± 2.8	117
$\mathcal{S}_8$: Contreventements†	NA	NA	13.4 ± 2.1	61
$\mathcal{S}_9$: Trottoir	NA	NA	11.6 ± 0.9	112
$\mathcal{S}_{11}$: Autres éléments	NA	NA	18.9 ± 2.6	230
$\mathcal{S}_{12}$: Épaulements	NA	11.2 ± 7.6	NA	25
$\mathcal{S}_{13}$: Élément en élastomère	14.2 ± 1.3	NA	NA	42
$\mathcal{S}_{14}$: Acier structural - tablier	NA	NA	24.3 ± 1.6	25
$\mathcal{S}_{16}$: Butoirs	NA	NA	NA	4
$\mathcal{S}_{17}$: Glissière médiane	NA	NA	NA	11
$\mathcal{S}_{18}$: Garde-fou	NA	NA	NA	11
$\mathcal{S}_{19}$: Acier structural - unités de fondation	NA	NA	NA	2
$\mathcal{S}_{20}$: Bande médiane	NA	NA	14.7 ± 4.9	6
$\mathcal{S}_{21}$: Portique d'extrémité	NA	NA	NA	6
$\mathcal{S}_{23}$: Acier structural - ptres triangulées	NA	NA	15.7 ± 5.8	8
$\mathcal{S}_{26}$: Toiture	NA	NA	13.7 ± 6.8	4
$\mathcal{S}_{27}$: Lambris	NA	NA	NA	11

NA: The results are not available due to limitations in the database.

Table C.4: Service-life (in years) before reaching the pre-intervention condition for the secondary categories of structural elements having underwent interventions h_3, with the maximum forecast period fixed at 120 years.

Structural Category $\mathcal{S}_m^{1:B,2}$	10$^{\text{th}}$ percentile	50$^{\text{th}}$ percentile	90$^{\text{th}}$ percentile
$\mathcal{S}_1$: Glissière (gauche ou droite)	NA	NA	NA
$\mathcal{S}_2$: Murs en aile / en retour	8	17	33
$\mathcal{S}_3$: Chasse-roue	6	16	39
$\mathcal{S}_4$: Glissières	NA	NA	NA
$\mathcal{S}_5$: Surface de roulement	6	16	42
$\mathcal{S}_6$: Diaphragmes	6	15	44
$\mathcal{S}_7$: Garde-grève	8	17	43
$\mathcal{S}_8$: Contreventements	12	20	41
$\mathcal{S}_9$: Trottoir	3	11	24
$\mathcal{S}_{11}$: Autres éléments	10	22	47
$\mathcal{S}_{12}$: Épaulements	NA	NA	NA
$\mathcal{S}_{13}$: Élément en élastomère	NA	NA	NA
$\mathcal{S}_{14}$: Acier structural - tablier	12	25	47
$\mathcal{S}_{16}$: Butoirs	NA	NA	NA
$\mathcal{S}_{17}$: Glissière médiane	NA	NA	NA
$\mathcal{S}_{18}$: Garde-fou	NA	NA	NA
$\mathcal{S}_{19}$: Acier structural - unités de fondation	NA	NA	NA
$\mathcal{S}_{20}$: Bande médiane	15	20	29
$\mathcal{S}_{21}$: Portique d'extrémité	NA	NA	NA
$\mathcal{S}_{23}$: Acier structural - poutres triangulées	10	29	41
$\mathcal{S}_{26}$: Toiture	NA	NA	NA
$\mathcal{S}_{27}$: Lambris	NA	NA	NA

NA: The results are not available due to limitations in the database.

References

[1] Adey, B. T. and Hajdin, R. (2011). Methodology for determination of financial needs of gradually deteriorating bridges with only structure level data. *Structure and Infrastructure Engineering*, 7(7-8):645–660 1573–2479.

[2] Agdas, D., Rice, J. A., Martinez, J. R., and Lasa, I. R. (2015). Comparison of visual inspection and structural-health monitoring as bridge condition assessment methods. *Journal of Performance of Constructed Facilities*, 30(3):04015049.

[3] Allah Bukhsh, Z., Stipanovic, I., Klanker, G., O'Connor, A., and Doree, A. G. (2019). Network level bridges maintenance planning using multi-attribute utility theory. *Structure and infrastructure engineering*, 15(7):872–885 1573–2479.

[4] Bar-Shalom, Y., Li, X. R., and Kirubarajan, T. (2004). *Estimation with applications to tracking and navigation: theory algorithms and software.* John Wiley Sons.

[5] Campbell, L. E., Connor, R. J., Whitehead, J. M., and Washer, G. A. (2019). Benchmark for evaluating performance in visual inspection of fatigue cracking in steel bridges. *Journal of Bridge Engineering*, 25(1):04019128

[6] Chase, S. B., Adu-Gyamfi, Y., Aktan, A., and Minaie, E. (2016). Synthesis of national and international methodologies used for bridge health indices. Technical report.

[7] Ferreira, C., Neves, L. C., Matos, J. C., and Soares, J. M. S. (2014). A degradation and maintenance model: Application to portuguese context. *Proceedings of Bridge Maintenance, Safety, Management and Life Extension*, pages 483–489.

[8] Fu, G. and Devaraj, D. (2008). *Methodology of Homogeneous and Non-homogeneous Markov Chains for Modelling Bridge Element Deterioration.* Michigan Department of Transportation.

[9] Ghodoosi, F., Bagchi, A., and Zayed, T. (2015). System-level deterioration model for reinforced concrete bridge decks. *Journal of Bridge Engineering*, 20(5):04014081

[10] Ghosn, M., Dueñas-Osorio, L., Frangopol, D., McAllister, T., Bocchini, P., Manuel, L., Ellingwood, B., Arangio, S., Bontempi, F., and Shah, M. (2016). Performance indicators for structural systems and infrastructure networks. *Journal of Structural Engineering*, 142(9):F4016003 0733–9445.

[11] Hamida, Z. and Goulet, J.-A. (2020a). Modeling infrastructure degradation from visual inspections using network-scale state-space models. *Structural Control and Health Monitoring*, pages 1545–2255.

[12] Hamida, Z. and Goulet, J.-A. (2020b). Network-scale deterioration modelling based on visual inspections and structural attributes. *Structural Safety*.

[13] Hamida, Z. and Goulet, J.-A. (2021). Quantifying the effects of interventions based on visual inspections of bridges network. *Structure and infrastructure engineering*, pages 1–12.

[14] Hastie, T., Tibshirani, R., Sherlock, G., Eisen, M., Brown, P., and Botstein, D. (1999). Imputing missing data for gene expression arrays. Technical report, Stanford University.

[15] Hooks, J. M. and Frangopol, D. M. (2013). Ltbp bridge performance primer. Technical report.

[16] Huang, Y.-H. (2010). Artificial neural network model of bridge deterioration. *Journal of Performance of Constructed Facilities*, 24(6):597–602

[17] Inkoom, S., Sobanjo, J. O., Thompson, P. D., Kerr, R., and Twumasi-Boakye, R. (2017). Bridge health index: Study of element condition states and importance weights. *Transportation Research Record*, 2612(1):67–75

[18] Jackson, C. H. (2011). Multi-state models for panel data: the msm package for r. *Journal of statistical software.*

[19] Kalbfleisch, J. and Lawless, J. F. (1985). The analysis of panel data under a markov assumption. *Journal of the American Statistical Association*, 80(392):863–871

[20] Kallen, M. and Van Noortwijk, J. (2006). Statistical inference for markov deterioration models of bridge conditions in the netherlands. In *Proceedings of the Third International Conference on Bridge Maintenance, Safety and Management*, number 16-19.

[21] Kalman, R. E. (1960). Contributions to the theory of optimal control. *Bol. Soc. Mat. Mexicana*, 5(2):102–119.

[22] Lee, J., Sanmugarasa, K., Blumenstein, M., and Loo, Y.-C. (2008). Improving the reliability of a bridge management system (bms) using an ann-based backward prediction model (bpm). *Automation in Construction*, 17(6):758–772

[23] Moore, M., Phares, B. M., Graybeal, B., Rolander, D., and Washer, G. (2001). Reliability of visual inspection for highway bridges, volume i. Technical report, Turner-Fairbank Highway Research Center, 6300 Georgetown Pike.

[24] MTQ (2014). *Manuel d'Inspection des Structures.* Ministère des Transports, de la Mobilité Durable et de l'Électrification des Transports.

[25] OBrien, E., Carey, C., and Keenahan, J. (2015). Bridge damage detection using ambient traffic and moving force identification. *Structural Control and Health Monitoring*, 22:1396–1407.

[26] Rauch, H. E., Striebel, C., and Tung, F. (1965). Maximum likelihood estimates of linear dynamic systems. *AIAA journal*, 3(8):1445–1450

[27] Runnalls, A. R. (2007). Kullback-leibler approach to gaussian mixture reduction. *IEEE Transactions on Aerospace and Electronic Systems*, 43(3):989–999

[28] Salmond, D. J. (1990). *Mixture reduction algorithms for target tracking in clutter*, volume 1305. International Society for Optics and Photonics.

[29] Simon, D. and Simon, D. L. (2010). Constrained kalman filtering via density function truncation for turbofan engine health estimation. *International Journal of Systems Science*, 41(2):159–171 0020–7721.

[30] Soetjipto, J. W., Adi, T. J. W., and Anwar, N. (2017). *Bridge Deterioration Prediction Model Based On Hybrid Markov-System Dynamic*, volume 138. EDP Sciences.

[31] Srikanth, I. and Arockiasamy, M. (2020). Deterioration models for prediction of remaining useful life of timber and concrete bridges–a review. *Journal of traffic and transportation engineering (English edition)*

[32] Straub, D., Schneider, R., Bismut, E., and Kim, H.-J. (2020). Reliability analysis of deteriorating structural systems. Structural safety, 82:101877

[33] Strauss, A., Vidovic, A., Zambon, I., Dengg, F., Tanasic, N., and Matos, J. C. (2016). Performance indicators for roadway bridges. In Proceedings of the 8th International Conference on Bridge Maintenance, Safety and Management, IABMAS 2016.

[34] Tien, I. and Der Kiureghian, A. (2016). Algorithms for bayesian network modeling and reliability assessment of infrastructure systems. Reliability Engineering System Safety, 156:134–147 0951–8320.

[35] Van Erp, H. N. and Orcesi, A. D. (2018). The use of nested sampling for prediction of infrastructure degradation under uncertainty. Structure and Infrastructure Engineering, pages 1–11 1573–2479.

[36] Winn, E. K. (2011). *Artificial neural network models for the prediction of bridge deck condition ratings. Master's thesis, Michigan State University.*

[37] Zhang, W. and Wang, N. (2017). *Bridge network maintenance prioritization under budget constraint.* Structural safety, *67:96–104*

[38] Zhang, Y., Kim, C.-W., and Tee, K. F. (2017). *Maintenance management of offshore structures using markov process model with random transition probabilities.* Structure and Infrastructure Engineering, *13(8):1068–1080.*